Revisiting Generalized p-Laplacian Regularized Framelet GCNs: Convergence, Energy Dynamic and as Non-Linear Diffusion

Anonymous authors
Paper under double-blind review

Abstract

This paper presents a comprehensive theoretical analysis of the graph p-Laplacian regularized framelet network (pL-UFG) to establish a solid understanding of its properties. We conduct a convergence analysis on pL-UFG, addressing the gap in the understanding of its asymptotic behaviors. Further by investigating the generalized Dirichlet energy of pL-UFG, we demonstrate that the Dirichlet energy remains non-zero throughout convergence, ensuring the avoidance of over-smoothing issues. Additionally, we elucidate the energy dynamic perspective, highlighting the synergistic relationship between the implicit layer in pL-UFG and graph framelets. This synergy enhances the model's adaptability to both homophilic and heterophilic data. Notably, we reveal that pL-UFG can be interpreted as a generalized non-linear diffusion process, thereby bridging the gap between pL-UFG and differential equations on the graph. Importantly, these multifaceted analyses lead to unified conclusions that offer novel insights for understanding and implementing pL-UFG, as well as other graph neural network (GNN) models. Finally, based on our dynamic analysis, we propose two novel pL-UFG models with manually controlled energy dynamics. We demonstrate empirically and theoretically that our proposed models not only inherit the advantages of pL-UFG but also significantly reduce computational costs for training on large-scale graph datasets.

1 Introduction

Graph neural networks (GNNs) have exhibited remarkable performance in propagating and predicting for graph-structured data in various domains, including citation networks (Kipf & Welling, 2016), social networks (Chen et al., 2018), molecules (Duvenaud et al., 2015), and traffic networks (Cui et al., 2019), among others. Generally, GNN models can be categorized into two major types: spatial GNNs, such as MPNN (Gilmer et al., 2017), GAT (Veličković et al., 2018), and GIN (Xu et al., 2019), which propagate node features based on connectivity information; and spectral GNNs, including GCN (Kipf & Welling, 2016), ChebyNet (Defferrard et al., 2016), and BernNet (He et al., 2021), which apply filtering in the spectral domain by utilizing the graph Fourier transform. Wavelet-based graph representation learning (Dong, 2017; Hammond et al., 2011; Li et al., 2020; Wang & Deng, 2021; Xu et al., 2018a; Zheng et al., 2021; 2023; 2022; Zou et al., 2022), as a type of spectral-based GNN, enables multi-resolution filtering on graph signals, thereby offering improved signal representation by capturing features at different scales. Notably, graph framelets (Dong, 2017; Zheng et al., 2022) allow separate modeling of low-pass and high-pass signal information, and have been used to define graph convolution in works such as (Chen et al., 2022b; Zheng et al., 2021; 2022). Graph framelets provide greater flexibility in controlling the integration of information in the low-pass frequency domain and the distinction of information in the high-pass frequency domain, exhibiting robustness and efficiency. Consequently, they achieve state-of-the-art results in various graph learning tasks (Chen et al., 2022b; Yang et al., 2022; Zheng et al., 2021; Zhou et al., 2021; 2022; Zou et al., 2022).

In the realm of developing increasingly sophisticated Graph Neural Networks (GNNs), there has been a recent surge of interest in understanding the theoretical underpinnings of these models. A key focus has been on analyzing the GNN propagation process as a linear diffusion process on the graph, with and without a source

term, to investigate the GNN's asymptotic behavior, which directly relates to the issue of over-smoothing (Chamberlain et al., 2021b;c; Thorpe et al., 2022; Chen et al., 2022c). Additionally, researchers have explored the power of GNNs from the perspective of graph topology, examining concepts such as distinguishing power and energy dynamics (Bronstein et al., 2021; Wang & Zhang, 2022; Morris et al., 2019; Chen et al., 2022a; Di Giovanni et al., 2022; Han et al., 2022). Moreover, recent studies have framed the GNN learning process as a form of graph regularization (Zhou & Schölkopf, 2005; Fu et al., 2022; Shao et al., 2022; Chen et al., 2022c), demonstrating that explicit propagation in GNNs can be substituted with an implicit layer that derives the problem solution (Gu et al., 2020; Liu et al., 2021). While the underlying connections among these theoretical aspects of GNNs are still being explored, a comprehensive assessment of GNN properties through various perspectives is expected. Ideally, a unified framework will emerge to guide and enhance GNNs in both theoretical and practical contexts.

In this paper, our primary focus is on the graph framelet model, specifically the graph p-Laplacian regularized framelet network (pL-UFG) model, which is equipped with a p-Laplacian based implicit layer as proposed in Shao et al. (2022) (see Section 2 for the formulation). Our objective is to analyze pL-UFG from various perspectives, including convergence, asymptotic energy behavior, energy dynamics, and its relationship with existing diffusion models. To the best of our knowledge, these aspects have not been thoroughly explored in the context of p-Laplacian based multi-scaled GNNs, leaving notable knowledge gaps. Accordingly, we summarize our contribution as follows:

- We rigorously prove the convergence of pL-UFG, providing insights into the asymptotic behavior of the model. This analysis addresses a crucial gap in the understanding of GNN models regularized with p-Laplacian based energy regularizer.
- We show that by assigning the proper values of two key model parameters (denoted as μ and p) of pL-UFG based on our theoretical analysis, the (generalized) Dirichlet energy of the node feature produced from pL-UFG will never converge to 0; thus the inclusion of the implicit layer will prevent the model (graph framelet) from potential over-smoothing issue.
- We demonstrate how the implicit layer in pL-UFG interacts with the energy dynamics of the graph framelet. Furthermore, we prove that pL-UFG can adapt to both homophily and heterophily graphs, enhancing its versatility and applicability.
- Based on our theoretical results, we propose two generalized pL-UFG models with controlled model dynamics, namely pL-UFG low-frequency dominant model (pL-UFG-LFD) and pL-UFG high frequency dominant model (pL-UFG-HFD). we further show that with controllable model dynamics, the computational cost of pL-UFG is largely reduced, making our proposed model capable of handling large-scale graph datasets.
- We establish that the propagation mechanism within pL-UFG enables a generalized non-linear graph diffusion. The conclusions based on our analysis from different perspectives are unified at the end of the paper, suggesting a promising framework for evaluating other GNNs.
- We conduct extensive experiments to validate our theoretical claims. The empirical results not only confirm pL-UFG's capability to handle both homophily and heterophily graphs but also demonstrate that our proposed models achieve comparable or superior classification accuracy with reduced computational cost. These findings are consistent across commonly tested and large-scale graph datasets.

The remaining sections of this paper are structured as follows. Section 2 presents fundamental notations related to graphs, GNN models, graph framelets and pL-UFG. In Section 3, we conduct a theoretical analysis on pL-UFG, focusing on the aforementioned aspects. Specifically, Section 3.1 presents the convergence analysis, while Section 3.2 examines the behavior of the p-Laplacian based implicit layer through a generalized Dirichlet energy analysis. Furthermore, Section 3.3 demystifies the interaction between the implicit layer and graph framelets from an energy dynamic perspective. We provide our proposed models (pL-UFG-LFD and pL-UFG-HFD) in section 3.4. Lastly, in Section 3.5, we demonstrate that the iterative algorithm derived

from the implicit layer is equivalent to a generalized non-linear diffusion process on the graph. Additionally, in Section 4 we further verify our theoretical claims by comprehensive numerical experiments. Lastly, in conclusion 5, we summarize the findings of this paper and provide suggestions for future research directions.

2 Preliminaries

In this section, we provide necessary notations and formulations utilized in this paper. We list the necessary notations with their meanings in the Table 1 below, although we will mention the meaning of them again when we first use them.

Table 1: Necessary notations

Notations	Brief Interpretation
$\mathbf{X}$	Initial node feature matrix
$\mathbf{F}^{(k)}$	Feature representation on k-th layer of GNN model
$\mathbf{f}(i)$	Individual row of $\mathbf{F}$
$\mathbf{F}_{i,:}$	One or more operation acts on each row of $\mathbf{F}$
$\mathbf{D}$	Graph degree matrix
$\widehat{\mathbf{A}}$	Normalized adjacency matrix
$\widetilde{\mathbf{L}}$	Normalized Laplacian matrix
$\mathbf{W}$	Graph weight matrix
$\mathcal{W}$	Framelet decomposition matrix
$\mathcal{I}$	Index set of all framelet decomposition matrices.
$\widehat{\mathbf{W}}$	Learnable weight matrix in GNN models
$\widetilde{\mathbf{W}}$,$\mathbf{\Omega}$,$\widehat{\mathbf{W}}$	Learnable weight matrices in defining generalized Dirichlet energy
$\mathbf{E}^{PF}(\mathbf{F})$	Generalized Dirichlet energy for implicit layer
$\mathbf{E}^{Fr}(\mathbf{F})$	Generalized framelet Dirichlet energy
$\mathbf{E}^{total}(\mathbf{F})$	Total generalized Dirichlet energy
$\{\lambda_i, \mathbf{u}_i\}_{i=1}^N$	Eigen-pairs of $\widetilde{\mathbf{L}}$

We also provide essential background information on the developmental history before the formulation of certain models, serving as a concise introduction to the related works.

Graph, Graph Convolution and Graph Consistency We denote a weighted graph as $\mathcal{G} = (\mathcal{V}, \mathcal{E}, \mathbf{W})$ with nodes set $\mathcal{V} = \{v_1, v_2, \cdots, v_N\}$ of total N nodes, edge set $\mathcal{E} \subseteq \mathcal{V} \times \mathcal{V}$ and graph adjacency matrix $\mathbf{W}$, where $\mathbf{W} = [w_{i,j}] \in \mathbb{R}^{N\times N}$ and $w_{i,j} = 1$ if $(v_i, v_j) \in \mathcal{E}$, else, $w_{i,j} = 0$. The nodes feature matrix is $\mathbf{X} \in \mathbb{R}^{N\times c}$ for $\mathcal{G}$ with each row $\mathbf{x}_i \in \mathbb{R}^c$ a feature vector associated with node v_i. For a matrix $\mathbf{A}$, we denote its transpose as $\mathbf{A}^\top$, and we use $[N]$ for set $\{1, 2, \ldots, N\}$. Throughout this paper, we will only focus on the undirect graph and use matrix $\mathbf{A}$ and $\mathbf{W}$ interchangeably for graph adjacency matrix [1]. The normalized graph Laplacian is defined as $\widetilde{\mathbf{L}} = \mathbf{I} - \mathbf{D}^{-\frac{1}{2}}(\mathbf{W} + \mathbf{I})\mathbf{D}^{-\frac{1}{2}}$, where $\mathbf{D} = \mathrm{diag}(d_{1,1}, \ldots, d_{N,N})$ is a diagonal degree matrix, $d_{i,i} = \sum_{j=1}^N w_{i,j}$ for $i = 1, \ldots, N$, and $\mathbf{I}$ is the identity matrix. From spectral graph theory (Chung, 1997), we have $\widetilde{\mathbf{L}} \succeq 0$, i.e. $\widetilde{\mathbf{L}}$ is a positive semi-definite (SPD) matrix. Let λ_i for $i = 1, ..., n$ be the eigenvalues of $\widetilde{\mathbf{L}}$, also known as graph spectra, and $\lambda_i \in [0, 2]$. For any given graph, we let $\rho_{\widetilde{\mathbf{L}}}$ be the largest eigenvalue of $\widetilde{\mathbf{L}}$. Lastly, for any vector $\mathbf{x} = (x_1, ..., x_c) \in \mathbb{R}^c$, $\|\mathbf{x}\|_2 = (\sum_{i=1}^c x_i^2)^{\frac{1}{2}}$ is the L_2-norm of $\mathbf{x}$, and similarly, $\|\mathbf{M}\| := \|\mathbf{M}\|_F = (\sum_{i,j} m_{i,j}^2)^{\frac{1}{2}}$ is the matrix Frobenius norm of any matrix $\mathbf{M} = [m_{i,j}]$.

Graph convolution network (GCN) (Kipf & Welling, 2016) produces a layer-wise (node feature) propagation rule based on the information from the normalized adjacency matrix as:

$$\mathbf{F}^{(k+1)} = \sigma\big(\widehat{\mathbf{A}}\mathbf{F}^{(k)}\widehat{\mathbf{W}}^{(k)}\big), \tag{1}$$

[1] We initially set $\mathbf{W}$ as the graph adjacency matrix in align with the notations used in (Fu et al., 2022; Shao et al., 2022)

where $\mathbf{F}^{(k)}$ is the embedded node feature, $\widehat{\mathbf{W}}^{(k)}$ the weight matrix for channel mixing (Bronstein et al., 2021), and σ any activation function such as sigmoid. The superscript $^{(k)}$ indicates the quantity associated with layer k, and $\mathbf{F}^{(0)} = \mathbf{X}$. We write $\widehat{\mathbf{A}} = \mathbf{D}^{-\frac{1}{2}}(\mathbf{W} + \mathbf{I})\mathbf{D}^{-\frac{1}{2}}$, the normalized adjacency matrix of $\mathcal{G}$. It is easy to see that the operation conducted in GCN before activation can be interpreted as a localized filter by the graph Fourier transform, i.e., $\mathbf{f}^{(k+1)} = \mathbf{U}^\top(\mathbf{I}_n - \mathbf{\Lambda})\mathbf{U}\mathbf{f}^{(k)}$, where $\mathbf{f}^{(k)} = \mathbf{F}^{(k)}\widehat{\mathbf{W}}^{(k)}$ and $\mathbf{U}, \mathbf{\Lambda}$ are from the eigendecomposition $\widetilde{\mathbf{L}} = \mathbf{U}^\top\mathbf{\Lambda}\mathbf{U}$. In fact, $\mathbf{U}\mathbf{f}$ is known as the Fourier transform of graph signal $\mathbf{f}$.

Over the development of GNNs, most of GNNs are designed under the homophily assumption in which connected (neighbouring) nodes are more likely to share the same label. The recent work by Zhu et al. (2020) identified that the general topology GNN fails to obtain outstanding results on the graphs with different class labels and dissimilar features in their connected nodes, which induces the notion of so-call heterophilic graphs. The definition of homophilic and heterophilic graphs are given by:

Definition 1 (Homophily and Heterophily (Fu et al., 2022))**.** The homophily or heterophily of a network is used to define the relationship between labels of connected nodes. The level of homophily of a graph can be measured by $\mathcal{H}(\mathcal{G}) = \mathbb{E}_{i\in\mathcal{V}}[|\{j\}_{j\in\mathcal{N}_{i,y_i=y_i}}|/|\mathcal{N}_i|]$, where $|\{j\}_{j\in\mathcal{N}_{i,y_i=y_i}}|$ denotes the number of neighbours of $i \in \mathcal{V}$ that share the same label as i, i.e. $y_i = y_j$. $\mathcal{H}(\mathcal{G}) \to 1$ corresponds to strong homophily while $\mathcal{H}(\mathcal{G}) \to 0$ indicates strong heterophily. We say that a graph is a homophilic (heterophilic) graph if it has strong homophily (heterophily).

Graph Framelet Framelets are a type of wavelet frame used in the analysis and processing of signals on graphs. The first wavelet frame with a lifting scheme for graph analysis was presented in (Sweldens, 1998). As computational power increased, Hammond et al. (2011) proposed a framework for wavelet transformation on graphs using Chebyshev polynomials for approximations. Later, Dong (2017) developed tight framelets on graphs by approximating smooth functions with filtered Chebyshev polynomials.

Framelets have been applied to graph learning tasks with outstanding results, as demonstrated in (Zheng et al., 2021). They are capable of decomposing graph signals and re-aggregating them effectively, as shown in the study on graph noise reduction by Zhou et al. (2021). Combining framelets with singular value decomposition (SVD) has also made them applicable to directed graphs (Zou et al., 2022). Recently, Yang et al. (2022) suggested a simple method for building more versatile and stable framelet families, known as Quasi-Framelets. In this study, we will introduce graph framelets using the same architecture described in (Yang et al., 2022). To begin, we define the filtering functions for Quasi-framelets.

A set of $R+1$ positive filtering functions, denoted as $\mathcal{F} = g_0(\xi), g_1(\xi), ..., g_R(\xi)$, is considered as Quasi-Framelet scaling functions on the interval $[0, \pi]$. These functions adhere to the identity condition:

$$g_0(\xi)^2 + g_1(\xi)^2 + \cdots + g_R(\xi)^2 \equiv 1, \quad \forall \xi \in [0, \pi], \tag{2}$$

where g_0 descents from 1 to 0, while g_R ascends from 0 to 1 as the frequency increases within the spectral domain $[0, \pi]$. The purpose of g_0 is to regulate the highest frequency, g_R is employed to control the lowest frequency, while the remaining functions govern the frequencies lying between them.

The Quasi-Framelet signal transformation matrices is defined as:

$$\mathcal{W}_{0,J} = \mathbf{U}g_0(\frac{\mathbf{\Lambda}}{2^{m+J}}) \cdots g_0(\frac{\mathbf{\Lambda}}{2^m})\mathbf{U}^\top, \tag{3}$$

$$\mathcal{W}_{r,0} = \mathbf{U}g_r(\frac{\mathbf{\Lambda}}{2^m})\mathbf{U}^\top, \quad \text{for } r = 1, ..., R, \tag{4}$$

$$\mathcal{W}_{r,\ell} = \mathbf{U}g_r(\frac{\mathbf{\Lambda}}{2^{m+\ell}})g_0(\frac{\mathbf{\Lambda}}{2^{m+\ell-1}}) \cdots g_0(\frac{\mathbf{\Lambda}}{2^m})\mathbf{U}^\top, \tag{5}$$
$$\text{for } r = 1, ..., R, \ell = 1, ..., J,$$

for a given set of Quasi-Framelet functions $\mathcal{F}$ and a given level $J \geq 0$ on a graph $\mathcal{G} = (\mathcal{V}, \mathcal{E})$ with normalized graph Laplacian $\widetilde{\mathbf{L}}$. $\mathcal{W}_{0,J}$ is defined as the product of $J+1$ Quasi-Framelet scaling functions g_0 applied to the Laplacian $\widetilde{\mathbf{L}}$ at different scales, with $\mathbf{U}$ as the orthogonal spectral bases. $\mathcal{W}_{r,0}$ is defined as $g_r(\frac{\mathbf{\Lambda}}{2^m})$ applied to $\widetilde{\mathbf{L}}$, where m is the coarsest scale level which is the smallest value satisfying $2^{-m}\lambda_n \leq \pi$. For

$1 \leq r \leq R$ and $1 \leq \ell \leq J$, $\mathcal{W}_{r,\ell}$ is defined as the product of $J - \ell + 1$ Quasi-Framelet scaling functions g_0 and ℓ Quasi-Framelet scaling functions g_r applied to $\widetilde{\mathbf{L}}$.

The stacked matrix $\mathcal{W}$ is the concatenation of $\mathcal{W}_{0,J}$, $\mathcal{W}_{1,0}$, ..., $\mathcal{W}_{R,0}$, $\mathcal{W}_{1,1}$, ..., $\mathcal{W}_{R,J}$. It can be proven that $\mathcal{W}^T\mathcal{W} = \mathbf{I}$, which provides a signal decomposition and reconstruction process based on $\mathcal{W}$. This is referred to as the graph Quasi-Framelet transformation.

To reduce the computational cost of eigendecomposition for the graph Laplacians, Chebyshev polynomials can be used to approximate the Quasi-Framelet transformation matrices. The approximated transformation matrices are defined by replacing $g_r(\xi)$ in equation 3-equation 5 with Chebyshev polynomials $\mathcal{T}_r(\xi)$ of a fixed degree, which is typically set to 3. The Quasi-Framelet transformation matrices are defined in equation 4 - equation 5 can be approximated by,

$$\mathcal{W}_{0,J} \approx \mathcal{T}_0(\frac{1}{2^{m+J}}\widetilde{\mathbf{L}}) \cdots \mathcal{T}_0(\frac{1}{2^m}\widetilde{\mathbf{L}}), \tag{6}$$

$$\mathcal{W}_{r,0} \approx \mathcal{T}_r(\frac{1}{2^m}\widetilde{\mathbf{L}}), \quad \text{for } r = 1, ..., R, \tag{7}$$

$$\mathcal{W}_{r,\ell} \approx \mathcal{T}_r(\frac{1}{2^{m+\ell}}\widetilde{\mathbf{L}})\mathcal{T}_0(\frac{1}{2^{m+\ell-1}}\widetilde{\mathbf{L}}) \cdots \mathcal{T}_0(\frac{1}{2^m}\widetilde{\mathbf{L}}), \tag{8}$$
$$\text{for } r = 1, ..., R, \ell = 1, ..., J.$$

For given $\mathcal{G}(\mathcal{V}, \mathcal{E})$, we can explicitly show the propagation of the spectral framelet convolution (Zheng et al., 2021; 2022; Yang et al., 2022) as:

$$\mathbf{F}^{(k+1)} = \sigma\left(\sum_{(r,\ell)\in\mathcal{I}} \mathcal{W}_{r,\ell}^{\top}\text{diag}(\theta_{r,\ell})\mathcal{W}_{r,\ell}\mathbf{F}^{(k)}\widehat{\mathbf{W}}^{(k)}\right), \tag{9}$$

where $\theta_{r,\ell} \in \mathbb{R}^N$, $\widehat{\mathbf{W}}^{(k)}$ are learnable matrices for diagonal scaling and channel mixing (Zheng et al., 2022). Let $\mathcal{I} = \{(r, j) : r = 1, ..., R, \ell = 0, 1, ..., J\} \cup \{(0, J)\}$ be the index set for all framelet decomposition matrices. Since the framelet system provides a perfect reconstruction on the input graph signal (i.e., $\mathcal{W}^{\top}\mathcal{W} = \mathbf{I}$), instead of propagating the node feature information via frequency domains (as shown in equation 9), recent study (Chen et al., 2022b) has also consider deploying framelet based propagation via spatial (graph adjacency) domain, and the resulting so-called spatial framelet with its propagation rule (without activation) as:

$$\mathbf{F}^{(k+1)} = \mathcal{W}_{0,J}^{\top}\widehat{\mathbf{A}}\mathcal{W}_{0,J}\mathbf{F}^{(k)}\widehat{\mathbf{W}}_{0,J}^{(k)} + \sum_{r,\ell} \mathcal{W}_{r,\ell}^{\top}\widehat{\mathbf{A}}\mathcal{W}_{r,\ell}\mathbf{F}^{(k)}\widehat{\mathbf{W}}_{r,\ell}^{(k)}. \tag{10}$$

Unlike spectral framelet methods, which the weight matrix $\widehat{\mathbf{W}}$ is shared across different (filtered) frequency domains, spatial framelets methods assign different weight matrices $\widehat{\mathbf{W}}_{r,\ell}$ to each (filtered) spatial domain to produce the graph convolution.

Generalized p-Laplacian Regularized Framelet GCN In this part, we provide several additional definitions to formulate the model (pL-UFG) that we are interested to analyze. Specifically, one of the recent works Fu et al. (2022) considered assigning an adjustable p-Laplacian regularizer to the (discrete) graph regularization problem that is conventionally treated as a way of producing GNN outcomes (i.e., Laplacian smoothing) (Zhou & Schölkopf, 2005). In view of the fact that the classic graph Laplacian regularizer measures the graph signal energy along edges under L_2 metric, it would be beneficial if GNN training process can be regularized under L_p metric in order to adapt to different graph inputs. Following these pioneer works, Shao et al. (2022) further integrated graph framelet and a generalized p-Laplacian regularizer to develop the so-called generalized p-Laplacian regularized framelet model. It involves a regularization problem over the energy quadratic form induced from graph p-Laplacian. To show this, we start by defining graph gradient as follows:

Definition 2 (Graph Gradient (Zhou & Schölkopf, 2005))**.** Let $\mathcal{F}_{\mathcal{V}} := \{\mathbf{F}|\mathbf{F} : \mathcal{V} \to \mathbb{R}^d\}$ and $\mathcal{F}_{\mathcal{E}} := \{\mathbf{g}|\mathbf{g} : \mathcal{E} \to \mathbb{R}^d\}$ be the function space on nodes and edges, respectively. Given a graph $\mathcal{G} = (\mathcal{V}, \mathcal{E}, \mathbf{W})$ and a function

$\mathbf{F} \in \mathcal{F}_{\mathcal{V}}$, the graph gradient is an operator $\nabla_W : \mathcal{F}_{\mathcal{V}} \to \mathcal{F}_{\mathcal{E}}$ defined as for all $[i,j] \in \mathcal{E}$,

$$(\nabla_W \mathbf{F})([i,j]) := \sqrt{\frac{w_{i,j}}{d_{j,j}}}\mathbf{f}_j - \sqrt{\frac{w_{i,j}}{d_{i,i}}}\mathbf{f}_i, \tag{11}$$

where $\mathbf{f}_i$ and $\mathbf{f}_j$ are the signal vectors on nodes i and j, i.e., the rows of $\mathbf{F}$.

For simplicity, we denote $\nabla_W \mathbf{F}$ as $\nabla \mathbf{F}$ as the graph gradient. The definition of (discrete) graph gradient is analogized from the notion of gradient from the continuous space. Similarly, we can further define the so-called graph divergence:

Definition 3 (Graph Divergence (Zhou & Schölkopf, 2005))**.** Given a graph $\mathcal{G} = (\mathcal{V}, \mathcal{E}, W)$ and a function $\mathbf{F} : \mathcal{V} \to \mathbb{R}^d$, $\mathbf{g} : \mathcal{E} \to \mathbb{R}^d$, the graph divergence is an operator $\mathrm{div} : \mathcal{F}_{\mathcal{E}} \to \mathcal{F}_{\mathcal{V}}$ such that

$$\langle \nabla \mathbf{F}, \mathbf{g} \rangle = \langle \mathbf{F}, -\mathrm{div}(\mathbf{g}) \rangle. \tag{12}$$

Furthermore, the graph divergence can be computed by:

$$\mathrm{div}(\mathbf{g})(i) = \sum_{j=1}^{N} \sqrt{\frac{w_{i,j}}{d_{i,i}}}(\mathbf{g}[i,j] - \mathbf{g}[j,i]). \tag{13}$$

With the formulation of graph gradient and divergence we are ready to define the graph p-Laplacian operator and the corresponding p-Dirichlet form (Zhou & Schölkopf, 2005; Fu et al., 2022) that serves as the regularizer in the model developed in (Shao et al., 2022). The graph p-Laplacian can be defined as follows:

Definition 4 (Graph p-Laplacian)**.** Given a graph $\mathcal{G} = (\mathcal{V}, \mathcal{E}, \mathbf{W})$ and a multiple channel signal function $\mathbf{F} : \mathcal{V} \to \mathbb{R}^d$, the graph p-Laplacian is an operator $\Delta_p : \mathcal{F}_{\mathcal{V}} \to \mathcal{F}_{\mathcal{V}}$, defined by:

$$\Delta_p \mathbf{F} := -\frac{1}{2}\mathrm{div}(\|\nabla \mathbf{F}\|^{p-2} \nabla \mathbf{F}), \quad \text{for } p \geq 1. \tag{14}$$

where $\|\cdot\|^{p-2}$ is element-wise power over the node gradient $\nabla \mathbf{F}$.

The corresponding p-Dirichlet form can be denoted as:

$$\mathcal{S}_p(\mathbf{F}) = \frac{1}{2} \sum_{(v_i, v_j) \in \mathcal{E}} \left\| \sqrt{\frac{w_{i,j}}{d_{j,j}}}\mathbf{f}_j - \sqrt{\frac{w_{i,j}}{d_{i,i}}}\mathbf{f}_i \right\|^p, \tag{15}$$

where we adopt the definition of element-wise p-norm as (Fu et al., 2022). It is not difficult to verify that once we set $p = 2$, we recover the graph Dirichlet energy (Zhou & Schölkopf, 2005) that is widely used to measure the difference between node features along the GNN propagation process.

Remark 1 (Dirichlet Energy, Graph Homophily and Heterophily)**.** Graph Dirichlet energy (Fu et al., 2022; Bronstein et al., 2021) has became a commonly applied measure of variation between node features via GNNs. It has been shown that once the graph is highly heterophily where the connected nodes are not likely to share identical labels, one may prefer GNNs that exhibit nodes feature sharpening effect, thus increasing Dirichlet energy, such that the final classification output of the connected nodes from these GNNs tend to be different. Whereas, when the graph is highly homophily, a smoothing effect (thus a decrease of Dirichlet energy) is preferred.

Shao et al. (2022) further generalized the p-Dirichlet form in equation 15 as:

$$\begin{aligned} \mathcal{S}_p(\mathbf{F}) &= \frac{1}{2} \sum_{(v_i, v_j) \in \mathcal{E}} \|\nabla_W \mathbf{F}([i,j])\|^p \\ &= \frac{1}{2} \sum_{v_i \in \mathcal{V}} \left[\left(\sum_{v_j \sim v_i} \|\nabla_W \mathbf{F}([i,j])\|^p \right)^{\frac{1}{p}} \right]^p = \frac{1}{2} \sum_{v_i \in \mathcal{V}} \|\nabla_W \mathbf{F}(v_i)\|_p^p, \end{aligned} \tag{16}$$

where $v_j \sim v_i$ stands for the node v_j that is connected to node v_i and $\nabla_W \mathbf{F}(v_i) = (\nabla_W \mathbf{F}([i,j]))_{v_j:(v_i,v_j)\in\mathcal{E}}$ is the node gradient vector for each node v_i and $\|\cdot\|_p$ is the vector p-norm. Moreover, we can further generalize the regularizer $\mathcal{S}_p(\mathbf{F})$ by considering any positive convex function ϕ as:

$$\mathcal{S}_p^{\phi}(\mathbf{F}) = \frac{1}{2}\sum_{v_i\in\mathcal{V}} \phi(\|\nabla_W \mathbf{F}(v_i)\|_p). \tag{17}$$

There are many choices of ϕ and p. When $\phi(\xi) = \xi^p$, we recover the p-Laplacian regularizer. Interestingly, by setting $\phi(\xi) = \xi^2$, we recover the so-called Tikhonov regularization which is frequently applied in image processing. When $\phi(\xi) = \xi$, i.e. identity map written as id, and $p = 1$, $\mathcal{S}_1^{id}(\mathbf{F})$ becomes the classic total variation regularization. Last but not the least, $\phi(\xi) = r^2\log(1+\xi^2/r^2)$ gives nonlinear diffusion. We note that there are many other choices on the form of ϕ. In this paper we will only focus on those mentioned in Shao et al. (2022) (i.e., the smooth ones).

The regularization problem proposed in Shao et al. (2022) is:

$$\mathbf{F} = \arg\min_{\mathbf{F}} \mathcal{S}_p^{\phi}(\mathbf{F}) + \mu\|\mathbf{F}-\mathbf{Y}\|_F^2. \tag{18}$$

An iterative algorithm is introduced in Shao et al. (2022) to address the above regularization problem in equation 18. The justification is summarized by the following proposition (Theorem 1 in Shao et al. (2022)):

Proposition 1. *For a given positive convex function $\phi(\xi)$, define*

$$\begin{aligned} M_{i,j} =& \frac{w_{i,j}}{2}\|\nabla_W \mathbf{F}([i,j])\|^{p-2}\cdot\left[\frac{\phi'(\|\nabla_W \mathbf{F}(v_i)\|_p)}{\|\nabla_W \mathbf{F}(v_i)\|_p^{p-1}} + \frac{\phi'(\|\nabla_W \mathbf{F}(v_j)\|_p)}{\|\nabla_W \mathbf{F}(v_j)\|_p^{p-1}}\right], \\ \alpha_{ii} =& 1/\left(\sum_{v_j\sim v_i}\frac{M_{i,j}}{d_{i,i}} + 2\mu\right), \qquad \beta_{ii} = 2\mu\alpha_{ii}, \end{aligned}$$

and denote the matrices $\mathbf{M} = [M_{i,j}]$, $\boldsymbol{\alpha} = diag(\alpha_{11},...,\alpha_{NN})$ and $\boldsymbol{\beta} = diag(\beta_{11},...,\beta_{NN})$. Then problem equation 18 can be solved by the following message passing process

$$\mathbf{F}^{(k+1)} = \boldsymbol{\alpha}^{(k)}\mathbf{D}^{-1/2}\mathbf{M}^{(k)}\mathbf{D}^{-1/2}\mathbf{F}^{(k)} + \boldsymbol{\beta}^{(k)}\mathbf{Y}, \tag{19}$$

with an initial value, e.g., $\mathbf{F}^{(0)} = \mathbf{0}$. Note, k denotes the discrete time index (iteration).

Equation 19 can be regarded as an implicit layer on the node features generated from graph framelet. Due to the extensive analysis conducted on the graph framelet's properties, our subsequent analysis will primarily concentrate on the iterative scheme presented in equation 19. However, we will also unveil the interaction between this implicit layer and the framelet in the following sections.

3 Theoretical Analysis of the pL-UFG

In this section, we will show detailed analysis on the convergence (Section 3.1) and energy behavior (Section 3.2) of the implicit layer presented in equation 19. In addition, we will also present some results regarding to the interaction between the implicit layer and graph framelet in Section 3.3 via the energy dynamic aspect based on the conclusion from Section 3.2. Lastly in Section 3.5, we will verify that the iterative algorithm induced from the p-Laplacian implicit layer admits a generalized non-linear diffusion process, thereby connecting the discrete iterative algorithm to the differential equations on graph.

First, we consider the form of matrix $\mathbf{M}$ in equation 19. Write

$$\zeta_{i,j}^{\phi}(\mathbf{F}) = \frac{1}{2}\left[\frac{\phi'(\|\nabla_W \mathbf{F}^{(k+1)}(v_i)\|_p)}{\|\nabla_W \mathbf{F}^{(k+1)}(v_i)\|_p^{p-1}} + \frac{\phi'(\|\nabla_W \mathbf{F}^{(k+1)}(v_j)\|_p)}{\|\nabla_W \mathbf{F}^{(k+1)}(v_j)\|_p^{p-1}}\right]. \tag{20}$$

$M_{i,j}$ can be simplified as

$$M_{i,j} = \zeta_{i,j}^{\phi}(\mathbf{F}) w_{i,j} \left\| \nabla_W \mathbf{F}([i,j]) \right\|^{p-2}. \tag{21}$$

$\zeta_{i,j}^{\phi}(\mathbf{F})$ is bounded as shown in the following lemma.

Lemma 1. *Assume*

$$\frac{\phi'(\xi)}{\xi^{p-1}} \leq C, \tag{22}$$

for a suitable constant C. We have $|\zeta_{i,j}^{\phi}(\mathbf{F})| \leq C$.

The proof is trivial thus we omit it here. In the sequel, we use $\zeta_{i,j}(\mathbf{F})$ for $\zeta_{i,j}^{\phi}(\mathbf{F})$ instead.

Remark 2. It is reasonable for assuming equation 22 in Lemma 1 so that $\zeta_{i,j}(\mathbf{F})$ is bounded. For example, one can easily verify that when $\phi(\xi) = \xi^p$, $\zeta_{i,j}(\mathbf{F})$ is bounded for all p. In particular, when $p = 2$, i.e., $\phi(\xi) = \xi^2$, we have $\frac{\phi'(\xi)}{\xi^{p-1}} = \frac{2\xi}{\xi^{p-1}} = 2\frac{\xi^2}{\xi^p}$, thus $\zeta_{i,j}(\mathbf{F})$ is bounded for all $0 < p \leq 2$. Furthermore, when $\phi(\xi) = \xi$, then $\frac{\phi'(\xi)}{\xi^{p-1}} = \frac{\xi}{\xi^{p-1}}$, indicating $\zeta_{i,j}(\mathbf{F})$ is bounded for all $0 < p \leq 1$. In addition, when $\phi(\xi) = \sqrt{\xi^2 + \epsilon^2} - \epsilon$, we have $\frac{\phi'(\xi)}{\xi^{p-1}} = \frac{(\xi^2+\epsilon^2)^{1/2}\xi}{\xi^{p-1}} \leq C\frac{\xi}{\xi^{p-1}}$. Therefore $\zeta_{i,j}(\mathbf{F})$ is bounded for all $0 < p \leq 2$. Lastly, when $\phi(\xi) = r^2 \log(1 + \frac{\xi^2}{r^2})$, the result of $\frac{\phi'(\xi)}{\xi^{p-1}}$ yields $r^2 \frac{1}{1+\frac{\xi^2}{r^2}} \cdot \frac{\frac{2}{r^2}\xi}{\xi^{p-1}} \leq 2\frac{\xi}{\xi^{p-1}}$. Hence $\zeta_{i,j}(\mathbf{F})$ remain bounded for all $0 < p \leq 2$. In summary, for all forms of ϕ we included in the model, $\zeta_{i,j}(\mathbf{F})$ is bounded.

The boundedness of $\zeta_{i,j}(\mathbf{F})$ from Lemma 1 is useful in the following convergence analysis.

3.1 Convergence Analysis of pL-UFG

We show the iterative algorithm presented in equation 19 will converge with a suitable choice of μ.

Theorem 1 (Week Convergence of the Proposed Model)**.** Given a graph $\mathcal{G}(\mathcal{V}, \mathcal{E}, \mathbf{W})$ with node features $\mathbf{X}$, if $\boldsymbol{\alpha}^{(k)}$, $\boldsymbol{\beta}^{(k)}$, $\mathbf{M}^{(k)}$ and $\mathbf{F}^{(k)}$ are updated according to equation 19, then there exist some real positive value μ, which depends on the input graph ($\mathcal{G}$, $\mathbf{X}$) and the quantity of p, updated in each iteration, such that:

$$\mathcal{L}_p^{\phi}(\mathbf{F}^{(k+1)}) \leq \mathcal{L}_p^{\phi}(\mathbf{F}^{(k)}),$$

where $\mathcal{L}_p^{\phi}(\mathbf{F}) := \arg\min_{\mathbf{F}} \mathcal{S}_p^{\phi}(\mathbf{F}) + \mu \|\mathbf{F} - \mathbf{Y}\|_F^2$.

Proof. First, write

$$M_{i,j}^{(k)} = \frac{w_{i,j}}{2} \left\| \nabla_W \mathbf{F}^{(k)}([i,j]) \right\|^{p-2} \cdot \left[\frac{\phi'(\|\nabla_W \mathbf{F}^{(k)}(v_i)\|_p)}{\|\nabla_W \mathbf{F}^{(k)}(v_i)\|_p^{p-1}} + \frac{\phi'(\|\nabla_W \mathbf{F}^{(k)}(v_j)\|_p)}{\|\nabla_W \mathbf{F}^{(k)}(v_j)\|_p^{p-1}} \right]. \tag{23}$$

The derivative of the regularization problem defined in equation 18 is:

$$\begin{aligned}
\left.\frac{\partial \mathcal{L}_p^{\phi}(\mathbf{F})}{\partial \mathbf{F}_{i,:}}\right|_{\mathbf{F}^{(k)}} =& 2\mu(\mathbf{F}_{i,:}^{(k)} - \mathbf{Y}_{i,:}) + \sum_{v_j \sim v_i} M_{ij}^{(k)} \frac{1}{\sqrt{d_{ii} w_{ij}}} \nabla_W \mathbf{F}^{(k)}([j,i]) \\
=& 2\mu(\mathbf{F}_{i,:}^{(k)} - \mathbf{Y}_{i,:}) + \sum_{v_j \sim v_i} M_{ij}^{(k)} \left(\frac{1}{d_{ii}} \mathbf{F}_{i,:}^{(k)} - \frac{1}{\sqrt{d_{ii} d_{jj}}} \mathbf{F}_{j,:}^{(k)} \right) \\
=& (2\mu + \sum_{v_j \sim v_i} M_{ij}^{(k)} / d_{ii}) \mathbf{F}_{i,:}^{(k)} - 2\mu \mathbf{Y}_{i,:} - \sum_{v_j \sim v_i} \frac{M_{ij}^{(k)}}{\sqrt{d_{ii} d_{jj}}} \mathbf{F}_{j,:}^{(k)} \\
=& \frac{1}{\alpha_{ii}^{(k)}} \mathbf{F}_{i,:}^{(k)} - \frac{1}{\alpha_{ii}^{(k)}} \left(\beta_{ii}^{(k)} \mathbf{Y}_{i,:} + \alpha_{ii}^{(k)} \sum_{v_j \sim v_i} \frac{M_{ij}^{(k)}}{\sqrt{d_{ii} d_{jj}}} \mathbf{F}_{j,:}^{(k)} \right)
\end{aligned} \tag{24}$$

Thus, according the update rule of $\mathbf{F}^{(k+1)}$ in equation 19, we have

$$\left.\frac{\partial \mathcal{L}_p^\phi(\mathbf{F})}{\partial \mathbf{F}_{i,:}}\right|_{\mathbf{F}^{(k)}} = \frac{\mathbf{F}_{i,:}^{(k)} - \mathbf{F}_{i,:}^{(k+1)}}{\alpha_{ii}^{(k)}}. \tag{25}$$

For our purpose, we denote the partial derivative at $\mathbf{F}^{(*)}$ of the objective function with respect to the node feature $\mathbf{F}_{i,;}$ as

$$\partial \mathcal{L}_p^\phi(\mathbf{F}_{i,:}^{(*)}) := \left.\frac{\partial \mathcal{L}_p^\phi(\mathbf{F})}{\partial \mathbf{F}_{i,:}}\right|_{\mathbf{F}^{(*)}} \tag{26}$$

For all $i, j \in [N]$, let $\mathbf{v} \in \mathbb{R}^{1\times c}$ be a disturbance acting on node i. Define the following:

$$\begin{aligned}
N_{i,j}^{(k)} &= W_{i,j}\left\|\sqrt{\frac{W_{i,j}}{D_{i,i}}}\mathbf{F}_{i,:}^{(k)} - \sqrt{\frac{W_{i,j}}{D_{j,j}}}\mathbf{F}_{j,:}^{(k)}\right\|^{p-2} \\
N_{i,j}'^{(k)} &= W_{i,j}\left\|\sqrt{\frac{W_{i,j}}{D_{i,i}}}(\mathbf{F}_{i,:}^{(k)} + \mathbf{v}) - \sqrt{\frac{W_{i,j}}{D_{j,j}}}\mathbf{F}_{j,:}^{(k)}\right\|^{p-2} \\
M_{i,j}^{(k)} &= N_{ij}^{(k)}\zeta_{i,j}(\mathbf{F}^{(k)}), \quad M_{i,j}'^{(k)} = N_{ij}'^{(k)}\zeta_{i,j}(\mathbf{F}^{(k)} + \mathbf{v}) \\
\alpha_{ii}'^{(k)} &= 1/\left(\sum_{v_j\sim v_i}\frac{M_{i,j}'^{(k)}}{D_{i,i}} + 2\mu\right), \qquad \beta_{ii}'^{(k)} = 2\mu\alpha_{ii}'^{(k)} \\
\mathbf{F}_{i,:}'^{(k+1)} &= \alpha_{i,i}'^{(k)}\sum_{v_j\sim v_i}\frac{\mathbf{M}_{i,j}'^{(k)}}{\sqrt{D_{i,i}D_{j,j}}}\mathbf{F}_{j,:}^{(k)} + \boldsymbol{\beta}'^{(k)}\mathbf{Y}_{i,:},
\end{aligned} \tag{27}$$

where $\zeta_{ij}(\mathbf{F})$ is defined as equation 20 and $\mathbf{F}^{(k)} + \mathbf{v}$ means that $\mathbf{v}$ only applies to the i-th of $\mathbf{F}^{(k)}$ [2].

Similar to equation 25, we compute

$$\partial \mathcal{L}_p^\phi(\mathbf{F}_{i,:}^{(k)} + \mathbf{v}) = \frac{1}{\alpha_{i,i}'^{(k)}}\left((\mathbf{F}_{i,:}^{(k)} + \mathbf{v}) - \mathbf{F}_{i,:}'^{(k+1)}\right). \tag{28}$$

Hence from both equation 25 and equation 28 we will have

$$\begin{aligned}
&\left\|\partial \mathcal{L}_p^\phi(\mathbf{F}_{i,:}^{(k)} + \mathbf{v}) - \partial \mathcal{L}_p^\phi(\mathbf{F}_{i,:}^{(k)})\right\| = \left\|\frac{1}{\alpha_{i,i}'^{(k)}}\left((\mathbf{F}_{i,:}^{(k)} + \mathbf{v}) - \mathbf{F}_{i,:}'^{(k+1)}\right) - \frac{1}{\alpha_{i,i}^{(k)}}\left(\mathbf{F}_{i,:}^{(k)} - \mathbf{F}_{i,:}^{(k+1)}\right)\right\| \\
\leq &\frac{1}{\alpha_{i,i}'^{(k)}}\|\mathbf{v}\| + \left\|\frac{1}{\alpha_{i,i}'^{(k)}}\left(\mathbf{F}_{i,:}^{(k)} - \mathbf{F}_{i,:}'^{(k+1)}\right) - \frac{1}{\alpha_{i,i}^{(k)}}\left(\mathbf{F}_{i,:}^{(k)} - \mathbf{F}_{i,:}^{(k+1)}\right)\right\| \\
= &\frac{1}{\alpha_{i,i}'^{(k)}}\|\mathbf{v}\| + \left\|\left(\frac{1}{\alpha_{i,i}'^{(k)}} - \frac{1}{\alpha_{i,i}^{(k)}}\right)\mathbf{F}_{i,:}^{(k)} - \frac{1}{\alpha_{i,i}'^{(k)}}\mathbf{F}_{i,:}'^{(k+1)} + \frac{1}{\alpha_{i,i}^{(k)}}\mathbf{F}_{i,:}^{(k+1)}\right\| \\
= &\frac{1}{\alpha_{i,i}'^{(k)}}\|\mathbf{v}\| + \left\|\sum_{v_j\sim v_i}\left(\frac{M_{i,j}'^{(k)}}{D_{i,i}} - \frac{M_{i,j}^{(k)}}{D_{i,i}}\right)\mathbf{F}_{i,:}^{(k)} - \sum_{v_j\sim v_i}\left(\frac{M_{i,j}'^{(k)}}{\sqrt{D_{i,i}D_{j,j}}}\right)\mathbf{F}_{j,:}'^{(k)} + \left(\frac{M_{i,j}^{(k)}}{\sqrt{D_{i,i}D_{j,j}}}\right)\mathbf{F}_{j,:}^{(k)}\right\| \\
= &\left(\sum_{v_j\sim v_i}\frac{M_{i,j}^{(k)}}{D_{i,i}} + 2\mu\right)\|\mathbf{v}\| + \sum_{v_j\sim v_i}\left(\frac{M_{i,j}'^{(k)} - M_{i,j}^{(k)}}{D_{i,i}}\right)\|\mathbf{v}\| \\
&+ \left\|\sum_{v_j\sim v_i}\left(\frac{M_{i,j}'^{(k)} - M_{i,j}^{(k)}}{D_{i,i}}\right)\mathbf{F}_{i,:}^{(k)} - \sum_{v_j\sim v_i}\left(\frac{M_{i,j}'^{(k)} - M_{i,j}^{(k)}}{\sqrt{D_{i,i}D_{j,j}}}\right)\mathbf{F}_{j,:}^{(k)}\right\|.
\end{aligned}$$

[2] With slightly abuse of notation, we denote N' as the matrix after assigning the disturbance $\mathbf{v}$ to the matrix N.

Note that in equation 27, $\|\cdot\|^{p-2}$ is the matrix L_2 norm raised to power $p-2$, that is $\|\mathbf{X}\|^{p-2} = \left((\sum_{i,j} x_{i,j}^2)^{\frac{1}{2}}\right)^{p-2}$. It is known that the matrix L_2 norm as a function is Lipschitz (Paulavičius & Žilinskas, 2006), so is its exponential to $p-2$. Furthermore, it is easy to verify that the function $\|\mathbf{N}' - \mathbf{N}\| \leq c\|\mathbf{v}\|$ and thus Lipschitz due to the property of $\mathbf{N}$ and $\mathbf{N}'$.

Hence, according to Lemma 1, the following holds

$$|M_{i,j}'^{(k)} - M_{i,j}^{(k)}| \leq C|N_{i,j}'^{(k)} - N_{i,j}^{(k)}| \leq C'\|\mathbf{v}\|.$$

Combining all the above, we have

$$\left\|\partial\mathcal{L}_p^\phi(\mathbf{F}_{i,:}^{(k)} + \mathbf{v}) - \partial\mathcal{L}_p^\phi(\mathbf{F}_{i,:}^{(k)})\right\| \leq \left(\sum_{v_j \sim v_i} \frac{M_{i,j}^{(k)}}{D_{i,i}} + 2\mu + o(\mathcal{G}, \mathbf{v}, \mathbf{X}, p)\right)\|\mathbf{v}\|, \tag{29}$$

where $o(\mathcal{G}, \mathbf{v}, \mathbf{X}, p)$ is bounded. It is worth noting that the quantity of $o(\mathcal{G}, \mathbf{v}, \mathbf{X}, p)$ is bounded by

$$\sum_{v_j \sim v_i}\left(\frac{M_{i,j}'^{(k)} - M_{i,j}^{(k)}}{D_{i,i}}\right)\|\mathbf{v}\| + \left\|\sum_{v_j \sim v_i}\left(\frac{M_{i,j}'^{(k)} - M_{i,j}^{(k)}}{D_{i,i}}\right)\mathbf{F}_{i,:}^{(k)} - \sum_{v_j \sim v_i}\left(\frac{M_{i,j}'^{(k)} - M_{i,j}^{(k)}}{\sqrt{D_{i,i}D_{j,j}}}\right)\mathbf{F}_{j,:}^{(k)}\right\|.$$

Let $\overline{o} = o(\mathcal{G}, \mathbf{v}, \mathbf{X}, p)$, $\boldsymbol{\gamma} = \{\gamma_1, ...\gamma_N\}^\top$, and $\boldsymbol{\eta} \in \mathbb{R}^{N\times c}$. By the Taylor expansion theorem we have:

$$\begin{aligned}
&\mathcal{L}_p^\phi(\mathbf{F}_{i,:}^{(k)} + \gamma_i\boldsymbol{\eta}_{i,:}) = \mathcal{L}_p^\phi(\mathbf{F}_{i,:}^{(k)}) + \gamma_i\int_0^1 \langle\partial\mathcal{L}_p^\phi(\mathbf{F}_{i,:}^{(k)} + \epsilon\gamma_i\boldsymbol{\eta}_{i,:}), \boldsymbol{\eta}_{i,:}\rangle d\epsilon \quad \forall i \\
&= \mathcal{L}_p^\phi(\mathbf{F}_{i,:}^{(k)}) + \langle\partial\mathcal{L}_p^\phi(\mathbf{F}_{i,:}^{(k)}), \boldsymbol{\eta}_{i,:}\rangle + \gamma_i\int_0^1 \left\langle\partial\mathcal{L}_p^\phi\left(\mathbf{F}_{i,:}^{(k)} + \epsilon\gamma_i\boldsymbol{\eta}_{i,:} - \partial\mathcal{L}_p^\phi\left(\mathbf{F}_{i,:}^{(k)}\right)\right), \boldsymbol{\eta}_{i,:}\right\rangle d\epsilon \\
&\leq \mathcal{L}_p^\phi(\mathbf{F}_{i,:}^{(k)}) + \langle\partial\mathcal{L}_p^\phi(\mathbf{F}_{i,:}^{(k)}), \boldsymbol{\eta}_{i,:}\rangle\gamma_i + \gamma_i\int_0^1 \left\|\partial\mathcal{L}_p^\phi\left(\mathbf{F}_{i,:}^{(k)} + \epsilon\gamma_i\boldsymbol{\eta}_{i,:} - \partial\mathcal{L}_p^\phi\left(\mathbf{F}_{i,:}^{(k)}\right)\right)\right\|\|\boldsymbol{\eta}_{i,:}\| d\epsilon \\
&\leq \mathcal{L}_p^\phi(\mathbf{F}_{i,:}^{(k)}) + \langle\partial\mathcal{L}_p^\phi(\mathbf{F}_{i,:}^{(k)}), \boldsymbol{\eta}_{i,:}\rangle\gamma_i + \left(\frac{1}{\alpha_{i,i}^{(k)}} + \overline{o}\right)\gamma_i^2\|\boldsymbol{\eta}_{i,:}\|^2
\end{aligned}$$

where the last inequality comes from equation 29.

Taking $\gamma_i = \alpha_{ii}^{(k)}$ and $\boldsymbol{\eta}_{i,:} = -\partial\mathcal{L}_p^\phi(\mathbf{F}_{i,:}^{(k)})$ in the above inequality gives

$$\begin{aligned}
&\mathcal{L}_p^\phi\left(\mathbf{F}_{i,:}^{(k)} - \alpha_{ii}^{(k)}\partial\mathcal{L}_p^\phi(\mathbf{F}_{i,:}^{(k)})\right) \\
\leq&\mathcal{L}_p^\phi(\mathbf{F}_{i,:}^{(k)}) - \alpha_{ii}^{(k)}\left\langle\partial\mathcal{L}_p^\phi(\mathbf{F}_{i,:}^{(k)}), \partial\mathcal{L}_p^\phi(\mathbf{F}_{i,:}^{(k)})\right\rangle + \frac{1}{2}\left(\frac{1}{\alpha_{i,i}^{(k)}} + \overline{o}\right)\alpha_{i,i}^{2(k)}\|\partial\mathcal{L}_p^\phi(\mathbf{F}_{i,:}^{(k)})\|^2 \\
=&\mathcal{L}_p^\phi(\mathbf{F}_{i,:}^{(k)}) - \frac{1}{2}\alpha_{i,i}^{(k)}\left(1 - \alpha_{i,i}^{(k)}\overline{o}\right)\|\partial\mathcal{L}_p^\phi(\mathbf{F}_{i,:}^{(k)})\|^2.
\end{aligned} \tag{30}$$

Given that $\overline{o}$ is bounded, if we choose a large μ, e.g., $2\mu > \overline{o}$, we will have

$$1 - \alpha_{i,i}^{(k)}\overline{o} = 1 - \frac{\overline{o}}{\sum_{v_j \sim v_i}\frac{M_{i,j}^{(k)}}{D_{i,i}} + 2\mu} > 0.$$

Thus the second term in equation 30 is positive. Hence we have

$$\mathcal{L}_p^\phi(\mathbf{F}_{i,:}^{(k+1)}) := \mathcal{L}_p^\phi\left(\mathbf{F}_{i,:}^{(k)} - \alpha_{ii}^{(k)}\partial\mathcal{L}_p^\phi(\mathbf{F}_{i,:}^{(k)})\right) \leq \mathcal{L}_p^\phi(\mathbf{F}_{i,:}^{(k)}).$$

This completes the proof. □

Theorem 1 shows that with suitable choice of the value of μ, the implicit layer is guaranteed to coverage. This inspires us to explore further on the variation of the node feature produced from implicit layer asymptotically. Recall that to measure the difference between node features, one common choice is to analyze its Dirichlet energy, which is initially considered in the setting $p = 2$ in equation 15. It is known that the Dirichlet energy of the node feature tend to approach to 0 after sufficiently large number of iterations in many GNN models (Kipf & Welling, 2016; Wu et al., 2020; Chamberlain et al., 2021a; Di Giovanni et al., 2022), known as over-smoothing problem. However, as we will show in the next section, by taking large μ or small p, the iteration from the implicit layer will always lift up the Dirichlet energy of the node features, and over-smoothing issue can be resolved completely in pL-UFG.

3.2 Energy Behavior of the pL-UFG

In this section, we show the energy behavior of the p-Laplacian based implicit layer. Specifically, we are interested in analyzing the property of the generalized Dirichlet energy defined in (Bronstein et al., 2021). We start with generalized graph convolution as follows:

$$\mathbf{F}^{(k+\tau)} = \mathbf{F}^{(k)} + \tau\sigma\left(-\mathbf{F}^{(k)}\mathbf{\Omega}^{(k)} + \widehat{\mathbf{A}}\mathbf{F}^{(k)}\widehat{\mathbf{W}}^{(k)} - \mathbf{F}^{(0)}\widetilde{\mathbf{W}}^{(k)}\right), \tag{31}$$

where $\mathbf{\Omega}^{(k)}$,$\widehat{\mathbf{W}}^{(k)}$ and $\widetilde{\mathbf{W}}^{(k)} \in \mathbb{R}^{c\times c}$ act on each node feature vector independently and perform channel mixing. When $\tau = 1$, and $\mathbf{\Omega}^{(k)} = \widetilde{\mathbf{W}}^{(k)} = \mathbf{0}$, it returns to GCN (Kipf & Welling, 2016). Additionally, by setting $\mathbf{\Omega}^{(k)} \neq 0$, we have the anisotropic instance of GraphSAGE (Xu et al., 2019). The expression of the generalized graph convolution further induces a class of generalized Dirichlet energy (Bronstein et al., 2021). Specifically, in this work, we consider a class of energy that is analogized from equation 31, that is:

$$\mathbf{E}(\mathbf{F}) = \frac{1}{2}\sum_i \langle \mathbf{f}_i, \mathbf{\Omega}\mathbf{f}_i\rangle - \frac{1}{2}\sum_{i,j}\widehat{\mathbf{A}}_{i,j}\langle \mathbf{f}_i, \widehat{\mathbf{W}}\mathbf{f}_j\rangle + \varphi^{(0)}(\mathbf{F}, \mathbf{F}^{(0)}). \tag{32}$$

It is worth noting that by setting $\mathbf{\Omega} = \widehat{\mathbf{W}} = \mathbf{I}_c$ and $\varphi^{(0)} = 0$, we recover the Dirichlet energy with $p = 2$ in equation 15. Additionally, we can set $\varphi^{(0)} = \sum_i \langle \mathbf{f}_i, \widetilde{\mathbf{W}}\mathbf{f}_i^{(0)}\rangle$, and rewrite equation 32 as:

$$\mathbf{E}(\mathbf{F}) = \left\langle \mathrm{vec}(\mathbf{F}), \frac{1}{2}(\mathbf{\Omega}\otimes\mathbf{I}_N - \widehat{\mathbf{W}}\otimes\widehat{\mathbf{A}})\mathrm{vec}(\mathbf{F}) + (\widetilde{\mathbf{W}}\otimes\mathbf{I}_N)\mathrm{vec}(\mathbf{F}^{(0)})\right\rangle. \tag{33}$$

Recall that equation 19 produces the node feature $\mathbf{F}^{(k+1)}$ according to the edge diffusion $\boldsymbol{\alpha}\mathbf{D}^{-1/2}\mathbf{M}\mathbf{D}^{-1/2}$ on $\mathbf{F}^{(k)}$ and the scaled source term $2\mu\boldsymbol{\alpha}\mathbf{F}^{(0)}$. Therefore, for each iteration in equation 19, we can define a layer-wise Dirichlet energy analogizing from equation 33. Specifically, one can achieve this by setting $\mathbf{\Omega} = \widehat{\mathbf{W}} = \widetilde{\mathbf{W}} = \mathbf{I}_c$, replacing the edge *diffusion* $\widehat{\mathbf{A}}$ by $\boldsymbol{\alpha}\mathbf{D}^{-1/2}\mathbf{M}\mathbf{D}^{-1/2}$ and the identity matrix $\mathbf{I}_N$ in the residual term by the diagonal matrix $2\mu\boldsymbol{\alpha}$. This generalized Dirichlet energy for the node features $\mathbf{F}^{(k+1)}$ in equation 19 is then:

$$\begin{aligned}\mathbf{E}^{PF}(\mathbf{F}^{(k+1)}) = \Big\langle &\mathrm{vec}(\mathbf{F}^{(k+1)}),\\ &\frac{1}{2}\left(\mathbf{I}_c\otimes\mathbf{I}_N - \mathbf{I}_c\otimes\left(\boldsymbol{\alpha}^{(k+1)}\mathbf{D}^{-1/2}\mathbf{M}^{(k+1)}\mathbf{D}^{-1/2}\right)\right)\mathrm{vec}(\mathbf{F}^{(k+1)}) + (\mathbf{I}_c\otimes 2\mu\boldsymbol{\alpha}^{(k+1)})\mathrm{vec}(\mathbf{F}^{(0)})\Big\rangle.\end{aligned} \tag{34}$$

where the superscript "^{PF}" is short for p-Laplacian based framelet. It is worth noting that once we set $\boldsymbol{\alpha}^{(k+1)}\mathbf{D}^{-1/2}\mathbf{M}^{(k+1)}\mathbf{D}^{-1/2}$ to a constant normalized adjacency matrix $\widehat{\mathbf{A}}$, and excluding the residual term,

we recover the Dirichlet energy ($\mathcal{S}_2(\mathbf{F})$ in equation 15) since

$$\begin{aligned}
\mathbf{E}^{PF}(\mathbf{F}^{(k+1)}) &= \left\langle \mathrm{vec}(\mathbf{F}^{(k+1)}), \frac{1}{2}\left(\mathbf{I}_c \otimes \mathbf{I}_N - \mathbf{I}_c \otimes \widehat{\mathbf{A}}\right)\mathrm{vec}(\mathbf{F}^{(k+1)})\right\rangle, \\
&= \left\langle \mathrm{vec}(\mathbf{F}^{(k+1)}), \frac{1}{2}\left(\mathbf{I}_c \otimes \widetilde{\mathbf{L}}\right)\mathrm{vec}(\mathbf{F}^{(k+1)})\right\rangle \\
&= \frac{1}{2}\mathrm{Tr}\left((\mathbf{F}^{(k+1)})^\top \widetilde{\mathbf{L}}\mathbf{F}^{(k+1)}\right) = \frac{1}{2}\sum_{i=1}^{N}\sum_{j=1}^{N}\left\|\sqrt{\frac{W_{i,j}}{D_{j,j}}}\mathbf{f}^{(k+1)}(j) - \sqrt{\frac{W_{i,j}}{D_{i,i}}}\mathbf{f}^{(k+1)}(i)\right\|^2 = \mathcal{S}_2(\mathbf{F}^{(k+1)}).
\end{aligned} \tag{35}$$

Where we denote the rows of $\mathbf{F}^{(k+1)}$ as $\mathbf{f}^{(k+1)}(i)$. With all these settings, we are now able to analyze the energy ($\mathbf{E}^{PF}(\mathbf{F})$) behavior of the pL-UFG, concluded as the following proposition:

Proposition 2 (Energy Behavior)**.** *Assume $\mathcal{G}$ is connected and unweighted. There exists sufficiently large value of μ or small value of p such that $\mathbf{E}^{PF}(\mathbf{F})$ will not converge to 0.*

Proof. Based on the form of $\mathbf{M}$, $\boldsymbol{\alpha}$ and $\boldsymbol{\beta}$, one can further show $\mathbf{E}^{PF}(\mathbf{F}^{(k+1)})$ in terms of the inner product between $\mathrm{vec}(\mathbf{F}^{(k+1)})$ and $\mathrm{vec}(\mathbf{F}^{(0)})$ as:

$$\begin{aligned}
&\mathbf{E}^{PF}(\mathbf{F}^{(k+1)}) = \Big\langle \mathrm{vec}(\mathbf{F}^{(k+1)}), \\
&\frac{1}{2}\left(\mathbf{I}_c \otimes \mathbf{I}_N - \mathbf{I}_c \otimes \left(\boldsymbol{\alpha}^{(k+1)}\mathbf{D}^{-1/2}\mathbf{M}^{(k+1)}\mathbf{D}^{-1/2}\right)\right)\mathrm{vec}(\mathbf{F}^{(k+1)}) + (\mathbf{I}_c \otimes 2\mu\boldsymbol{\alpha}^{(k+1)})\mathrm{vec}(\mathbf{F}^{(0)})\Big\rangle, \qquad (36) \\
&= \Big\langle \mathrm{vec}(\mathbf{F}^{(k+1)}), \frac{1}{2}\left(\mathbf{I}_c \otimes \mathbf{I}_N - \mathbf{I}_c \otimes \left(\boldsymbol{\alpha}^{(k+1)}\mathbf{D}^{-1/2}\mathbf{M}^{(k+1)}\mathbf{D}^{-1/2}\right)\right)\mathrm{vec}\left(\boldsymbol{\alpha}^{(k)}\mathbf{D}^{-1/2}\mathbf{M}^{(k)}\mathbf{D}^{-1/2}\mathbf{F}^{(k)} + 2\mu\boldsymbol{\alpha}^{(k)}\mathbf{F}^{(0)}\right) \\
&+(\mathbf{I}_c \otimes 2\mu\boldsymbol{\alpha}^{(k+1)})\mathrm{vec}(\mathbf{F}^{(0)})\Big\rangle, \\
&= \Big\langle \mathrm{vec}(\mathbf{F}^{(k+1)}), \frac{1}{2}\left(\mathbf{I}_c \otimes \mathbf{I}_N - \mathrm{vec}\left(\left(\boldsymbol{\alpha}^{(k+1)}\mathbf{D}^{-1/2}\mathbf{M}^{(k+1)}\mathbf{D}^{-1/2}\right)\left(\boldsymbol{\alpha}^{(k)}\mathbf{D}^{-1/2}\mathbf{M}^{(k)}\mathbf{D}^{-1/2}\mathbf{F}^{(k)} + 2\mu\boldsymbol{\alpha}^{(k)}\mathbf{F}^{(0)}\right)\right)\right) \\
&+(\mathbf{I}_c \otimes 2\mu\boldsymbol{\alpha}^{(k+1)})\mathrm{vec}(\mathbf{F}^{(0)})\Big\rangle \\
&= \Bigg\langle \mathrm{vec}(\mathbf{F}^{(k+1)}), \frac{1}{2}\Bigg(\mathbf{I}_c \otimes \mathbf{I}_N - \Bigg(\mathbf{I}_c \otimes \left(\prod_{s=0}^{k+1}\boldsymbol{\alpha}^{(s)}\mathbf{D}^{-1/2}\mathbf{M}^{(s)}\mathbf{D}^{-1/2}\right) \\
&+\sum_{s=0}^{k+1}\left(\prod_{l=k-s}^{k+1}\boldsymbol{\alpha}^{(l)}\mathbf{D}^{-1/2}\mathbf{M}^{(l)}\mathbf{D}^{-1/2}\right)\left(2\mu\boldsymbol{\alpha}^{(l-1)}\right) - 2\mu\boldsymbol{\alpha}^{(k+1)}\Bigg)\mathrm{vec}(\mathbf{F}^{(0)})\Bigg)\Bigg\rangle. \qquad (37)
\end{aligned}$$

Based on equation 36 and equation 37 , to have $\mathbf{E}^{PF}(\mathbf{F}^{(k+1)})$ increase, one needs to require [3]:

$$\mathbf{I}_c \otimes \left(\boldsymbol{\alpha}^{(k+1)}\mathbf{D}^{-1/2}\mathbf{M}^{(k+1)}\mathbf{D}^{-1/2}\right)\mathrm{vec}(\mathbf{F}^{(k+1)}) - (\mathbf{I}_c \otimes 2\mu\boldsymbol{\alpha}^{(k+1)})\mathrm{vec}(\mathbf{F}^{(0)}) < 0. \tag{38}$$

This then requires[4]:

$$\mathbf{I}_c \otimes \left(\prod_{s=0}^{k+1}\boldsymbol{\alpha}^{(s)}\mathbf{D}^{-1/2}\mathbf{M}^{(s)}\mathbf{D}^{-1/2} + \sum_{s=0}^{k+1}\left(\prod_{l=k-s}^{k+1}\boldsymbol{\alpha}^{(l)}\mathbf{D}^{-1/2}\mathbf{M}^{(l)}\mathbf{D}^{-1/2}\right)\left(2\mu\boldsymbol{\alpha}^{(l-1)}\right) - 2\mu\boldsymbol{\alpha}^{(k+1)}\right) < 0. \tag{39}$$

Note that the entries of the summation of the first two terms in the above equation are non-negative, and the last term $2\mu\boldsymbol{\alpha}^{(k+1)}$ is a diagonal matrix that only with non-zero entries. Referring to equation 37, to

[3] Strictly speaking, one shall further require all elements in $\mathbf{F}^{(k+1)}$ larger than or equal to 0. As this can be achieved by assigned a non-linear activation function (i.e., ReLU) to the framelet, we omit it here in our main analysis.

[4] In addition, we note that to thoroughly verify $\mathbf{E}^{PF}(\mathbf{F}^{(k+1)})$ is a type of energy, one needs to further require $\nabla^2(\mathbf{E}^{PF}(\mathbf{F}^{(k+1)})) = \mathbf{I}_c \otimes \mathbf{I}_N - \mathbf{I}_c \otimes \left(\prod_{s=0}^{k+1}\boldsymbol{\alpha}^{(s)}\mathbf{D}^{-1/2}\mathbf{M}^{(s)}\mathbf{D}^{-1/2}\right) + \sum_{s=0}^{k+1}\left(\prod_{l=k-s}^{k+1}\boldsymbol{\alpha}^{(l)}\mathbf{D}^{-1/2}\mathbf{M}^{(l)}\mathbf{D}^{-1/2}\right)\left(2\mu\boldsymbol{\alpha}^{(l-1)}\right) - 2\mu\boldsymbol{\alpha}^{(k+1)}$ to be symmetric, which can be verified by checking the symmetrical property of $\mathbf{M}$, $\boldsymbol{\alpha}$ and $\boldsymbol{\beta}$.

ensure an increase in $\mathbf{E}^{PF}(\mathbf{F}^{(k+1)})$, one shall require the quantify of μ sufficiently large such that the negative entries on the diagonal of

$$\left(\prod_{s=0}^{k+1}\boldsymbol{\alpha}^{(s)}\mathbf{D}^{-1/2}\mathbf{M}^{(s)}\mathbf{D}^{-1/2}+\sum_{s=0}^{k+1}\left(\prod_{l=k-s}^{k+1}\boldsymbol{\alpha}^{(l)}\mathbf{D}^{-1/2}\mathbf{M}^{(l)}\mathbf{D}^{-1/2}\right)\left(2\mu\boldsymbol{\alpha}^{(l-1)}\right)-2\mu\boldsymbol{\alpha}^{(k+1)}\right)$$

are sufficient small[5], resulting in the inner product in equation 37 being larger. To explicitly verify this, we take $k=0$ as an example, and our result can be easily generalized to any value of k.

When $k=0$, equation 39 becomes:

$$\begin{aligned}
&\mathbf{I}_c\otimes\left(\boldsymbol{\alpha}^{(1)}\mathbf{D}^{-1/2}\mathbf{M}^{(1)}\mathbf{D}^{-1/2}\right)\mathrm{vec}(\mathbf{F}^{(1)})-(\mathbf{I}_c\otimes 2\mu\boldsymbol{\alpha}^{(1)})\mathrm{vec}(\mathbf{F}^{(0)})\\
&=\mathbf{I}_c\otimes\left(\boldsymbol{\alpha}^{(1)}\mathbf{D}^{-1/2}\mathbf{M}^{(1)}\mathbf{D}^{-1/2}\right)\mathrm{vec}\left(\boldsymbol{\alpha}^{(0)}\mathbf{D}^{-1/2}\mathbf{M}^{(0)}\mathbf{D}^{-1/2}\mathbf{F}^{(0)}+2\mu\boldsymbol{\alpha}^{(0)}\mathbf{F}^{(0)}\right)-(\mathbf{I}_c\otimes 2\mu\boldsymbol{\alpha}^{(1)})\mathrm{vec}(\mathbf{F}^{(0)}),\\
&=\mathbf{I}_c\otimes\left(\boldsymbol{\alpha}^{(1)}\mathbf{D}^{-1/2}\mathbf{M}^{(1)}\mathbf{D}^{-1/2}\right)\left(\mathbf{I}_c\otimes\left(\boldsymbol{\alpha}^{(0)}\mathbf{D}^{-1/2}\mathbf{M}^{(0)}\mathbf{D}^{-1/2}+2\mu\boldsymbol{\alpha}^{(0)}\right)\mathrm{vec}(\mathbf{F}^{(0)})\right)-(\mathbf{I}_c\otimes 2\mu\boldsymbol{\alpha}^{(1)})\mathrm{vec}(\mathbf{F}^{(0)}),\\
&=\mathbf{I}_c\otimes\left(\prod_{s=0}^{1}\boldsymbol{\alpha}^{(s)}\mathbf{D}^{-1/2}\mathbf{M}^{(s)}\mathbf{D}^{-1/2}+\left(\boldsymbol{\alpha}^{(1)}\mathbf{D}^{-1/2}\mathbf{M}^{(1)}\mathbf{D}^{-1/2}2\mu\boldsymbol{\alpha}^{(0)}\right)-2\mu\boldsymbol{\alpha}^{(1)}\right)\mathrm{vec}(\mathbf{F}^{(0)}).
\end{aligned}\tag{40}$$

$\left(\prod_{s=0}^{1}\boldsymbol{\alpha}^{(s)}\mathbf{D}^{-1/2}\mathbf{M}^{(s)}\mathbf{D}^{-1/2}+\left(\boldsymbol{\alpha}^{(1)}\mathbf{D}^{-1/2}\mathbf{M}^{(1)}\mathbf{D}^{-1/2}2\mu\boldsymbol{\alpha}^{(0)}\right)-2\mu\boldsymbol{\alpha}^{(1)}\right)$ computes as:

$$\begin{aligned}
&\prod_{s=0}^{1}\alpha_{i,i}^{(s)}D_{i,i}^{-1/2}M_{i,j}^{(s)}D_{j,j}^{-1/2}+\left(\alpha_{i,i}^{(1)}D_{i,i}^{-1/2}M_{i,j}^{(1)}D_{j,j}^{-1/2}2\mu\alpha_{i,i}^{(0)}\right)-2\mu\alpha_{i,i}^{(1)}\\
&=\prod_{s=0}^{1}\left[\left(1/\left(\sum_{v_j\sim v_i}\frac{M_{i,j}^{(s)}}{D_{i,i}}+2\mu\right)\right)\left(\frac{\left\|\nabla_W\mathbf{F}^{(s)}([i,j])\right\|^{p-2}}{\sqrt{D_{i,i}D_{j,j}}}\right)\right]+\\
&\left[\left(1/\left(\sum_{v_j\sim v_i}\frac{M_{i,j}^{(1)}}{D_{i,i}}+2\mu\right)\right)\left(\frac{\left\|\nabla_W\mathbf{F}^{(1)}([i,j])\right\|^{p-2}}{\sqrt{D_{i,i}D_{j,j}}}\right)\left(2\mu/\left(\sum_{v_j\sim v_i}\frac{M_{i,j}^{(0)}}{D_{i,i}}+2\mu\right)\right)\right]\\
&-\left(2\mu/\left(\sum_{v_j\sim v_i}\frac{M_{i,j}^{(1)}}{D_{i,i}}+2\mu\right)\right),\\
&=\left(\frac{\left\|\nabla_W\mathbf{F}^{(0)}([i,j])\right\|^{p-2}}{\left(\sum_{v_j\sim v_i}\frac{M_{i,j}^{(0)}}{D_{i,i}}+2\mu\right)\cdot\sqrt{D_{i,i}D_{j,j}}}\right)\left(\frac{\left\|\nabla_W\mathbf{F}^{(1)}([i,j])\right\|^{p-2}}{\left(\sum_{v_j\sim v_i}\frac{M_{i,j}^{(1)}}{D_{i,i}}+2\mu\right)\cdot\sqrt{D_{i,i}D_{j,j}}}\right)+\\
&\left(\frac{\left\|\nabla_W\mathbf{F}^{(1)}([i,j])\right\|^{p-2}}{\left(\sum_{v_j\sim v_i}\frac{M_{i,j}^{(1)}}{D_{i,i}}+2\mu\right)\cdot\sqrt{D_{i,i}D_{j,j}}}\cdot 2\mu/\left(\sum_{v_j\sim v_i}\frac{M_{i,j}^{(0)}}{D_{i,i}}+2\mu\right)\right)-\left(2\mu/\left(\sum_{v_j\sim v_i}\frac{M_{i,j}^{(1)}}{D_{i,i}}+2\mu\right)\right).
\end{aligned}\tag{41}$$

Now we see that by assigning a sufficient large of μ or small value of p, we have both first two terms in equation 41 approach to 0 as well as the third term $\frac{\left\|\nabla_W\mathbf{F}^{(1)}([i,j])\right\|^{p-2}}{\left(\sum_{v_j\sim v_i}\frac{M_{i,j}^{(1)}}{D_{i,i}}+2\mu\right)\cdot\sqrt{D_{i,i}D_{j,j}}}\approx 0$. Additionally, we have both $2\mu/\left(\sum_{v_j\sim v_i}\frac{M_{i,j}^{(0)}}{D_{i,i}}+2\mu\right)$ and $2\mu/\left(\sum_{v_j\sim v_i}\frac{M_{i,j}^{(1)}}{D_{i,i}}+2\mu\right)\approx 1$. Therefore, the summation result of

[5]It is not difficult to verify that this condition is equivalent to requiring that the matrix $\mathbf{Q}=\left(\left(\boldsymbol{\alpha}^{(k+1)}\mathbf{D}^{-1/2}\mathbf{M}^{(k+1)}\mathbf{D}^{-1/2}\right)\mathrm{vec}(\mathbf{F}^{(k+1)})-(\mathbf{I}_c\otimes 2\mu\boldsymbol{\alpha}^{(k+1)})\mathrm{vec}(\mathbf{F}^{(0)})\right)$ must contain negative eigenvalue(s). We note that similar condition has been proposed in (Di Giovanni et al., 2022) in order to make GNN models induce high frequency dominant energy dynamic to fit the heterophilic graph input.

equation 41 tends to be 0 and the entries of the resulting matrix of equation 41 tend to be negative. Based on equation 37, there will be an increase of the node Dirichlet energy. More precisely, when there is a sufficiently large quantity of μ or small value of p we have:

$$\mathbf{E}^{PF}(\mathbf{F}^{(k+1)}) \approx \left\langle \mathrm{vec}(\mathbf{F}^{(k+1)}), \frac{1}{2}\left(\mathbf{I}_c \otimes \left(2\mu\boldsymbol{\alpha}^{(k+1)} + \mathbf{I}_N\right)\right)\mathrm{vec}(\mathbf{F}^{(0)})\right\rangle, \tag{42}$$

and it is clear to see that the large/small quantity of μ (or small/large value of p) is capable of amplifying/shrinking the Dirichlet energy. Furthermore, it is worth noting that we have only show an increase of Dirichlet energy in terms of $\mathbf{F}^{(0)}$, while the conclusion we reached does not suggest there will always be an increase of Dirichlet energy between each iteration in equation 19. Finally the conclusion can be easily generalized to any iteration and this completes the proof. □

Remark 3. Proposition 2 shows that regardless of the framelet convolution, the p-Laplacian based implicit layer will not generate identical node feature across graph nodes, and thus the so-called over-smoothing issue will not appear **asymptotically**. Furthermore, it is worth noting that the result from Proposition 2 provides the theoretical justification of the empirical observations in (Shao et al., 2022), where a large value of μ or small value of p is suitable for fitting heterophily datasets which commonly require the output of GNN to have higher Dirichlet energy.

3.3 Interaction with Framelet Energy Dynamic

To analyze the interaction between the energy dynamic of framelet convolution and the p-Laplacian based implicit propagation, We first briefly review some recent work on the energy dynamic of the GNNs. In (Di Giovanni et al., 2022), the propagation of GNNs was considered as the gradient flow of the Dirichlet energy that can be formulated as:

$$\mathbf{E}(\mathbf{F}) = \frac{1}{2}\sum_{i=1}^{N}\sum_{j=1}^{N}\left\|\sqrt{\frac{W_{i,j}}{D_{j,j}}}\mathbf{f}(j) - \sqrt{\frac{W_{i,j}}{D_{i,i}}}\mathbf{f}(i)\right\|^2, \tag{43}$$

and similarly by setting the power from 2 to p, we recover the p-Dirichlet form presented in equation 15. The gradient flow of the Dirichlet energy yields the so-called graph heat equation (Chung, 1997) as $\dot{\mathbf{F}}^{(k)} = -\nabla\mathbf{E}(\mathbf{F}^{(k)}) = -\widetilde{\mathbf{L}}\mathbf{F}^{(k)}$. Its Euler discretization leads to the propagation of linear GCN models (Wu et al., 2019a; Wang et al., 2021). The process is called Laplacian smoothing (Li et al., 2018) and it converges to the kernel of $\widetilde{\mathbf{L}}$, i.e., $\ker(\widetilde{\mathbf{L}})$ as $k \to \infty$, resulting in non-separation of nodes with same degrees, known as the over-smoothing issue.

Following this observation, the work (Han et al., 2022; Di Giovanni et al., 2022) also show even with the help of the non-linear activation function and the weight matrix via classic GCN equation 1, the process described is still dominated by the low frequency (small Laplacian eigenvalues) of the graph, hence eventually converging to the kernel of $\widetilde{\mathbf{L}}$, for almost every initialization. To quantify such behavior, Di Giovanni et al. (2022); Han et al. (2022) consider a general dynamic as $\dot{\mathbf{F}}^{(k)} = \mathrm{GNN}_\theta(\mathbf{F}^{(k)}, k)$, with $\mathrm{GNN}_\theta(\cdot)$ as an arbitrary graph neural network function, and also characterizes its behavior by low/high-frequency-dominance (L/HFD).

Definition 1 ((Di Giovanni et al., 2022))**.** $\dot{\mathbf{F}}^{(k)} = \mathrm{GNN}_\theta(\mathbf{F}^{(k)}, k)$ is Low-Frequency-Dominant (LFD) if $\mathbf{E}\big(\mathbf{F}^{(k)}/\|\mathbf{F}^{(k)}\|\big) \to 0$ as $k \to \infty$, and is High-Frequency-Dominant (HFD) if $\mathbf{E}\big(\mathbf{F}^{(k)}/\|\mathbf{F}^{(k)}\|\big) \to \rho_{\widetilde{\mathbf{L}}}/2$ as $t \to \infty$.

Lemma 2 ((Di Giovanni et al., 2022))**.** *A GNN model is LFD (resp. HFD) if and only if for each $t_j \to \infty$, there exists a sub-sequence indexed by $k_{j_l} \to \infty$ and $\mathbf{H}_\infty$ such that $\mathbf{F}(k_{j_l})/\|\mathbf{F}(k_{j_l})\| \to \mathbf{F}_\infty$ and $\widetilde{\mathbf{L}}\mathbf{H}_\infty = 0$ (resp. $\widetilde{\mathbf{L}}\mathbf{H}_\infty = \rho_{\widetilde{\mathbf{L}}}\mathbf{F}_\infty$).*

Remark 4 (LFD, HFD and graph homophily)**.** Based on Definition 1 and Lemma 2, for a given GNN model, if $\mathcal{G}$ is homophilic, i.e., adjacency nodes are more likely to share the same label, one may prefer the model can induce a LFD dynamic in order to fit the characteristic of $\mathcal{G}$. On the other hand, if $\mathcal{G}$ is heterophilic, the model is expected to induce a HFD dynamic, so that even in the adjacent nodes, their predicted labels still tend to be different. Thus, ideally, a model should be flexible enough to accommodate both LFD and HFD dynamics.

Generalized from the energy dynamic framework provided in (Di Giovanni et al., 2022), Han et al. (2022) develops a framelet Dirichlet energy and analyzed the energy behavior of both spectral (equation 9) and spatial framelet (equation 10) convolutions. Specifically, let $\mathbf{E}^{Fr}_{r,\ell}(\mathbf{F}) = \frac{1}{2}\mathrm{Tr}\big((\mathcal{W}_{r,\ell}\mathbf{F})^\top \mathcal{W}_{r,\ell}\mathbf{F}\mathbf{\Omega}_{r,\ell}\big) - \frac{1}{2}\mathrm{Tr}\big((\mathcal{W}_{r,\ell}\mathbf{F})^\top \mathrm{diag}(\theta)_{r,\ell}\mathcal{W}_{r,\ell}\mathbf{F}\widehat{\mathbf{W}}\big)$ for all $(r,\ell) \in \mathcal{I}$. The total framelet generalized energy is given by

$$\begin{aligned}\mathbf{E}^{Fr}_{r,\ell}(\mathbf{F}) &= \mathbf{E}^{Fr}_{0,J}(\mathbf{F}) + \sum_{r,\ell}\mathbf{E}^{Fr}_{r,\ell}(\mathbf{F}) \\ &= \frac{1}{2}\sum_{(r,\ell)\in\mathcal{I}}\left\langle \mathrm{vec}(\mathbf{F}), \left(\mathbf{\Omega}_{r,\ell}\otimes \mathcal{W}^\top_{r,\ell}\mathcal{W}_{r,\ell} - \widehat{\mathbf{W}}\otimes \mathcal{W}^\top_{r,\ell}\mathrm{diag}(\theta)_{r,\ell}\mathcal{W}_{r,\ell}\right)\mathrm{vec}(\mathbf{F})\right\rangle, \end{aligned} \tag{44}$$

where the superscript "Fr" stands for the framelet convolution, and this definition is based on the fact that the total Dirichlet energy is conserved under framelet decomposition (Han et al., 2022; Di Giovanni et al., 2022). By analyzing the gradient flow of the framelet energy [6] defined above, Han et al. (2022) concluded the energy dynamic of framelet as:

Proposition 3 ((Han et al., 2022))**.** *The spectral graph framelet convolution equation 9 with Haar-type filter can induce both LFD and HFD dynamics. Specifically, let $\boldsymbol{\theta}_{0,\ell} = \mathbf{1}_N$ and $\boldsymbol{\theta}_{r,\ell} = \theta\mathbf{1}_N$ for $r = 1, ..., L, \ell = 1, ..., J$ where $\mathbf{1}_N$ is a size N vector of all 1s. When $\theta \in [0, 1)$, the spectral framelet convolution is LFD and when $\theta > 1$, the spectral framelet convolution is HFD.*

It is worth noting that there are many other settings rather than $\boldsymbol{\theta}_{0,\ell} = \mathbf{1}_N$ and $\boldsymbol{\theta}_{r,\ell} = \theta\mathbf{1}_N$, i.e. adjusting θ, for inducing LFD/HFD from framelet. However, in this paper, we only consider the conditions described in Proposition 3. To properly compare the energy dynamics between the framelet models, we present the following definition.

Definition 2 (Stronger/Weaker Dynamic)**.** Let $\mathcal{Q}_\theta$ be the family of framelet models with the settings described in Proposition 3 and choice of θ. We say that one framelet model $\mathcal{Q}_{\theta_1}$ is with a stronger LFD than another framelet model $\mathcal{Q}_{\theta_2}$ if $\theta_1 < \theta_2$, and weaker otherwise. Similarly, we say $\mathcal{Q}_{\theta_1}$ is with a stronger HFD than $\mathcal{Q}_{\theta_2}$ if $\theta_1 > \theta_2$, and weaker otherwise [7].

Remark 5. Similar reasoning of Proposition 3 can be easily generalized to other commonly used framelet types such as Linear, Sigmoid and Entropy (Yang et al., 2022).

With all these settings, we summarize the interaction between framelet and p-Laplacian based implicit propagation as:

Lemma 3 (Stronger HFD)**.** *Based on the condition described in Proposition 3, when framelet is HFD, with sufficient large value of μ or small of p, the p-Laplacian implicit propagation further amplify the Dirichlet energy of the node feature produced from the framelets, and thus achieving a higher HFD dynamic than original framelet in equation 9.*

Proof. The proof can be done by verification. Recall that by setting sufficient large of μ or small of p, $\mathbf{E}^{PF}(\mathbf{F}^{(k+1)})$ in equation 42 has the form

$$\mathbf{E}^{PF}(\mathbf{F}^{(k+1)}) \approx \left\langle \mathrm{vec}(\mathbf{F}^{(k+1)}), \frac{1}{2}\left(\mathbf{I}_c \otimes \left(2\mu\boldsymbol{\alpha}^{(k+1)} + \mathbf{I}_N\right)\right)\mathrm{vec}(\mathbf{F}^{(0)})\right\rangle.$$

[6] Similar to the requirement on our p-Laplacian based framelet energy ($\mathbf{E}^{PF}(\mathbf{F}^{(k+1)})$, to thoroughly verify the framelet energy in equation 44 is a type of energy, we shall further require: $\nabla^2\mathbf{E}^{Fr}_{r,\ell}(\mathbf{F}) = \mathbf{\Omega}_{r,\ell}\otimes\mathcal{W}^\top_{r,\ell}\mathcal{W}_{r,\ell} - \widehat{\mathbf{W}}\otimes\mathcal{W}^\top_{r,\ell}\widetilde{\mathbf{L}}\mathcal{W}_{r,\ell}$ is symmetric, which can be satisfied by requiring both $\mathbf{\Omega}$ and $\widehat{\mathbf{W}}$ are symmetric.

[7] In case of any confusion, we note that in this paper we only compare the model's dynamics relationship when both of two (framelet) models are with the same frequency dominated dynamics (i.e., LFD, HFD).

Similarly, when framelet is HFD, with $\boldsymbol{\theta}_{0,\ell} = \mathbf{1}_N$, $\boldsymbol{\theta}_{r,\ell} = \theta \mathbf{1}_N$ and $\theta > 1$, the Dirichlet energy (of $\mathbf{F}^{(k+1)}$) equation 44 can be rewritten as:

$$\begin{aligned}\mathbf{E}^{Fr}_{r,\ell}(\mathbf{F}^{(k+1)}) &= \frac{1}{2}\sum_{(r,\ell)\in\mathcal{I}} \left\langle \mathrm{vec}(\mathbf{F}^{(k+1)}), \left(\boldsymbol{\Omega}_{r,\ell} \otimes \mathcal{W}^{\top}_{r,\ell}\mathcal{W}_{r,\ell} - \widehat{\mathbf{W}} \otimes \mathcal{W}^{\top}_{r,\ell}\mathrm{diag}(\theta)_{r,\ell}\mathcal{W}_{r,\ell}\right)\mathrm{vec}(\mathbf{F}^{(k+1)})\right\rangle, \\ &= \frac{1}{2}\sum_{(r,\ell)\in\mathcal{I}} \left\langle \mathrm{vec}(\mathbf{F}^{(k+1)}), \left(\widehat{\mathbf{W}} \otimes \left(\mathcal{W}^{\top}_{r,\ell}\mathcal{W}_{r,\ell} - \mathcal{W}^{\top}_{r,\ell}\mathrm{diag}(\theta)_{r,\ell}\mathcal{W}_{r,\ell}\right)\right)\mathrm{vec}(\mathbf{F}^{(k+1)})\right\rangle, \end{aligned} \tag{45}$$

where the last equality is achieved by letting $\boldsymbol{\Omega} = \widehat{\mathbf{W}}$, meaning that no external force [8] exist within the space that contains the node features. We note that it is reasonable to have such assumption in order to explicitly analyze the energy changes in equation 44 via the changes of θ. Now we take the Haar framelet with $\ell = 1$ as an example, meaning there will be only one high-pass and low-pass frequency domain in the framelet model. Specifically, the R.H.S of equation 45 can be further rewritten as:

$$\begin{aligned}&\frac{1}{2}\sum_{(r,\ell)\in\mathcal{I}} \left\langle \mathrm{vec}(\mathbf{F}^{(k+1)}), \left(\widehat{\mathbf{W}} \otimes \left(\mathcal{W}^{\top}_{r,\ell}\mathcal{W}_{r,\ell} - \mathcal{W}^{\top}_{r,\ell}\mathrm{diag}(\theta)_{r,\ell}\mathcal{W}_{r,\ell}\right)\right)\mathrm{vec}(\mathbf{F}^{(k+1)})\right\rangle \\ &\approx \frac{1}{2}\left\langle \mathrm{vec}(\mathbf{F}^{(k+1)}), \left(\widehat{\mathbf{W}} \otimes \left(\mathbf{I}_N - \mathcal{W}^{\top}_{1,1}\mathrm{diag}(\theta)_{1,1}\mathcal{W}_{1,1}\right)\right)\mathrm{vec}(\mathbf{F}^{(k+1)})\right\rangle. \end{aligned} \tag{46}$$

The inclusion of $\mathcal{W}^{\top}_{1,1}\mathrm{diag}(\theta)_{1,1}\mathcal{W}_{1,1}$ is based on the form of Haar type framelet with one scale. In addition, the approximation in equation 46 is due to the outcome of HFD [9]. Now we combine the framelet energy in the above equation (equation 46) with the energy induced from p-Laplacian based implicit propagation (equation 42). Denote the total energy induced from framelet and implicit layer as:

$$\begin{aligned}&\mathbf{E}^{(total)}(\mathbf{F}^{(k+1)}) = \\ &\frac{1}{2}\left\langle \mathrm{vec}(\mathbf{F}^{(k+1)}), \left(\left(\widehat{\mathbf{W}} \otimes \left(\mathbf{I}_N - \mathcal{W}^{\top}_{1,1}\mathrm{diag}(\theta)_{1,1}\mathcal{W}_{1,1}\right)\right)\mathrm{vec}(\mathbf{F}^{(k+1)}) + \mathbf{I}_c \otimes \left(2\mu\boldsymbol{\alpha}^{(k+1)} + \mathbf{I}_N\right)\mathrm{vec}(\mathbf{F}^{(0)})\right)\right\rangle. \end{aligned} \tag{47}$$

Obviously $\mathbf{E}^{(total)}(\mathbf{F}^{(k+1)})$ is larger than both $\mathbf{E}^{Fr}_{r,\ell}(\mathbf{F}^{(k+1)})$ (the framelet energy under HFD) and $\mathbf{E}^{PF}(\mathbf{F}^{(k+1)})$ (energy generated from the p-Laplacian layer). Hence we have verified that the implicit layer further amplifies the Dirichlet energy. Moreover, one can approximate this stronger dynamic by re-parameterizing $\mathbf{E}^{(total)}(\mathbf{F}^{(k+1)})$ by assigning a higher quantity of $\theta' > \theta > 0$ and excluding the residual term. Hence, the inclusion of the implicit layer induces a higher HFD dynamic to framelet, and that completes the proof. □

Corollary 1 (Escape from Over-smoothing Issue)**.** With the same conditions in Proposition 3, when framelet is LFD, the implicit layer (with sufficient large μ or small p) ensures the Dirichlet energy of node features does not converge to 0, thus preventing the model from the over-smoothing issue.

Proof. The proof can be done by combining Proposition 3 and Proposition 2, thus providing the alignment on the properties of pL-UFG from different aspects. □

Corollary 2 (Stronger LFD)**.** Based on the condition described in Proposition 3, when framelet is LFD, with sufficient small of μ or larger of p, the p-Laplacian implicit propagation further shrink the Dirichlet energy of the node feature produced from framelet, and thus achieving a stronger LFD dynamic.

Proof. The proof can be simply accomplished by applying the same reasoning in Lemma 3, we omit it here. □

[8] For details, please check (Bronstein et al., 2021)

[9] The result in equation 46 provides identical conclusion on the claim in (Di Giovanni et al., 2022) such that in order to have a HFD dynamic, $\widehat{\mathbf{W}}$ must have negative eigenvalue(s).

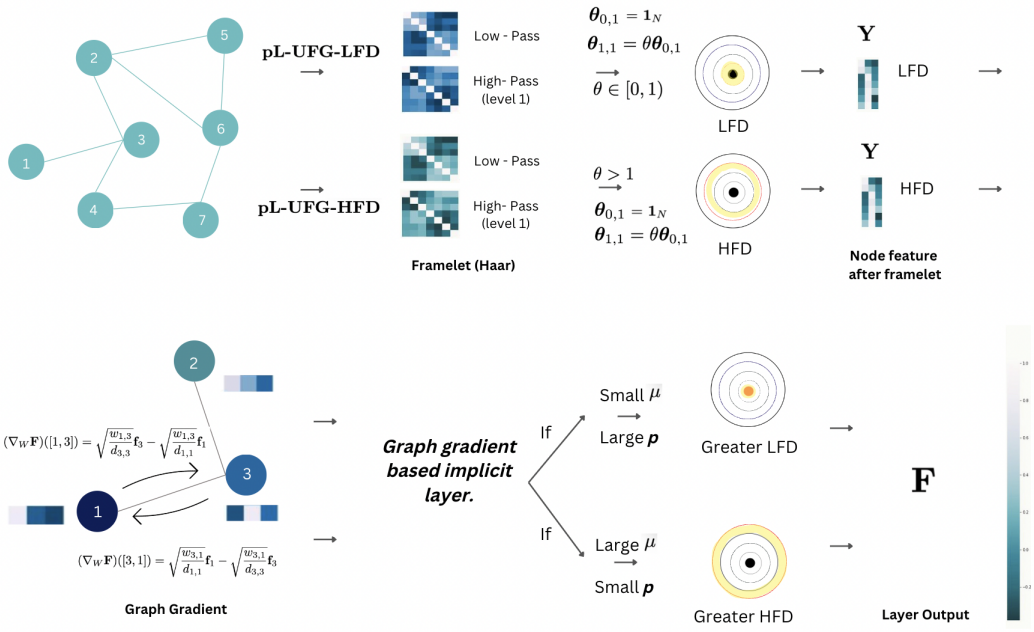

Figure 1: Illustration of the working flow of pL-UFG-LFD and pL-UFG-HFD under the Haar type frame with $\ell = 1$. The input graph features are first decomposed onto two frequency domains and further filtered by the diagonal matrix $\boldsymbol{\theta}_{0,1}$ and $\boldsymbol{\theta}_{1,1}$. With controlled model dynamics from Proposition 3 i.e., $\boldsymbol{\theta}_{0,1} = \mathbf{1}_N$ and $\boldsymbol{\theta}_{1,1} = \theta\boldsymbol{\theta}_{0,1}$, framelet can induce both LFD and HFD dynamics resulting as different level of Dirichlet energy of the produced node features. It is straightforward to check that when framelet is LFD, the level of node Dirichlet energy is less than its HFD counterpart. The generated node features from graph framelet is then inputted into p-Laplacian (with graph gradient as one component) based implicit layer. Based on our conclusions in Lemma 3 and Corollary 2 with small/large quantity of p and large/small quantity of μ, the model's (framelet) dynamics are further strengthened resulting even smaller/higher energy levels.

3.4 Proposed Model with Controlled Dynamics

Based on the aforementioned conclusions regarding energy behavior and the interaction between the implicit layer and framelet's energy dynamics, it becomes evident that irrespective of the homophily index of any given graph input, one can readily apply the condition of $\boldsymbol{\theta}$(s) in Proposition 3 to facilitate the adaptation of the pL-UFG model to the input graph by simply adjusting the quantities of μ and p. This adjustment significantly reduces the training cost of the graph framelet. For instance, consider the case of employing a Haar type frame with $\ell = 1$, where we have only one low-pass and one high-pass domain. In this scenario, the trainable matrices for this model are $\boldsymbol{\theta}_{0,1}$, $\boldsymbol{\theta}_{1,1}$, and $\widehat{\mathbf{W}}$. Based on our conclusions, we can manually set both $\boldsymbol{\theta}_{0,1}$ and $\boldsymbol{\theta}_{1,1}$ to our requested quantities, thereby inducing either LFD or HFD. Consequently, the only remaining training cost is associated with $\widehat{\mathbf{W}}$, leading to large reduction on the overall training cost while preserving model's capability of handling both types of graphs. Accordingly, we proposed two additional pL-UFG variants with controlled model dynamics, namely **pL-UFG-LFD** and **pL-UFG-HFD**.We note that to properly represent the Dirichlet energy of node features, we borrow the concept of electronic orbital energy levels in Figure. 1. The shaded outermost electrons correspond to higher energy levels, which can be analogously interpreted as higher variations in node features. Conversely, the closer the electrons are to the nucleus, the lower their energy levels, indicating lower variations in node features.

3.5 Equivalence to Non-Linear Diffusion

Diffusion on graph has gained its popularity recently (Chamberlain et al., 2021b; Thorpe et al., 2022) by providing a framework (i.e., PDE) to understand the GNNs architecture and as a principled way to develop a

broad class of new methods. To the best of our knowledge, although the GNNs based on linear diffusion on graph (Chamberlain et al., 2021b;a; Thorpe et al., 2022) have been intensively explored, models built from non-linear graph diffusion have not attracted much attention in general. In this section, we aim to verify that the iteration equation 19 admits a scaled nonlinear diffusion with a source term. To see this, recall that p-Laplacian operator defined in equation 14 has the form:

$$\Delta_p \mathbf{F} := -\frac{1}{2}\mathrm{div}(\|\nabla \mathbf{F}\|^{p-2}\nabla \mathbf{F}), \quad \text{for } p \geq 1. \tag{48}$$

Plugging in the definition of graph gradient and divergence defined in equation 11 and equation 13 into the above equation, one can compactly write out the form of p-Laplacian as:

$$(\Delta_p \mathbf{F})(i) = \sum_{v_j \sim v_i} \sqrt{\frac{W_{i,j}}{D_{i,i}}} \|\nabla_W \mathbf{F}([i,j])\|^{p-2} \left(\sqrt{\frac{W_{i,j}}{D_{i,i}}}\mathbf{f}(i) - \sqrt{\frac{W_{i,j}}{D_{j,j}}}\mathbf{f}(j) \right). \tag{49}$$

Furthermore, if we treat the iteration equation equation 19 as a diffusion process, its forward Euler scheme has the form:

$$\begin{aligned} \frac{\mathbf{F}^{(k+1)} - \mathbf{F}^{(k)}}{\tau} &= \boldsymbol{\alpha}^{(k)}\mathbf{D}^{-1/2}\mathbf{M}^{(k)}\mathbf{D}^{-1/2}\mathbf{F}^{(k)} - \mathbf{F}^{(k)} + \boldsymbol{\beta}^{(k)}\mathbf{Y}, \\ &= \left(\boldsymbol{\alpha}^{(k)}\mathbf{D}^{-1/2}\mathbf{M}^{(k)}\mathbf{D}^{-1/2} - \mathbf{I}\right)\mathbf{F}^{(k)} + \boldsymbol{\beta}^{(k)}\mathbf{Y}. \end{aligned} \tag{50}$$

We set $\tau = 1$ for the rest of analysis for the convenience reasons. With all these setups, we summarize our results in the following:

Lemma 4 (Non-Linear Diffusion)**.** *Assuming $\mathcal{G}$ is connected, the forward Euler scheme presented in equation 50 admits a generalized non-linear diffusion on the graph. Specifically, we have:*

$$\left(\boldsymbol{\alpha}^{(k)}\mathbf{D}^{-1/2}\mathbf{M}^{(k)}\mathbf{D}^{-1/2} - \mathbf{I}\right)\mathbf{F}^{(k)} + \boldsymbol{\beta}^{(k)}\mathbf{Y} = \boldsymbol{\alpha}\left(\mathrm{div}(\|\nabla \mathbf{F}^{(k)}\|^{p-2}\nabla \mathbf{F}^{(k)})\right) + 2\mu\boldsymbol{\alpha}^{(k)}\mathbf{D}\mathbf{F}^{(k)} + 2\mu\boldsymbol{\alpha}^{(k)}\mathbf{F}^{(0)}. \tag{51}$$

Proof. The proof can be done by verification. We can explicitly write out the computation on the i-th row of the left hand side of equation 51 as:

First let us denote the rows of $\mathbf{F}^{(k)}$ as $\mathbf{f}^{(k)}(i)$'s.

$$\begin{aligned} &\sum_{v_j \sim v_i} \left(\alpha_{i,i}^{(k)} D_{ii}^{-1/2} M_{i,j}^{(k)} D_{jj}^{-1/2}\right)\mathbf{f}^{(k)}(j) - \mathbf{f}^{(k)}(i) + \beta_{i,i}^{(k)} Y(i) \\ =&\alpha_{i,i}^{(k)} \left(\sum_{v_j \sim v_i} \left(\frac{M_{ij}}{\sqrt{D_{ii}}\sqrt{D_{jj}}}\mathbf{f}^{(k)}(j) \right) - \frac{1}{\alpha_{i,i}^{(k)}}\mathbf{f}^{(k)}(i) \right) + 2\mu\alpha_{i,i}^{(k)}\mathbf{f}^{(0)}(i) \\ =&\alpha_{i,i}^{(k)} \left(\sum_{v_j \sim v_i} \left(\frac{M_{ij}}{\sqrt{D_{ii}}\sqrt{D_{jj}}}\mathbf{f}^{(k)}(j) \right) - \sum_{v_j \sim v_i} \left(\frac{M_{ij}}{D_{ii}} + 2\mu \right)\mathbf{f}^{(k)}(i) \right) + 2\mu\alpha_{i,i}^{(k)}\mathbf{f}^{(0)}(i) \\ =&\alpha_{i,i}^{(k)} \left(\sum_{v_j \sim v_i} \sqrt{\frac{W_{i,j}}{D_{i,i}}} \|\nabla_W \mathbf{F}([i,j])\|^{p-2} \left(\sqrt{\frac{W_{i,j}}{D_{j,j}}}\mathbf{f}^{(k)}(j) - \sqrt{\frac{W_{i,j}}{D_{i,i}}}\mathbf{f}^{(k)}(i) \right) + 2\mu \sum_{v_j \sim v_i} \mathbf{f}^{(k)}(i) \right) \\ &+ 2\mu\alpha_{i,i}^{(k)}\mathbf{f}^{(0)}(i) \\ =&\alpha_{i,i}^{(k)} \left((\Delta_p \mathbf{F})(i) \right) + 2\mu\alpha_{i,i}^{(k)} D_{ii}\mathbf{f}^{(k)}(i) + 2\mu\alpha_{i,i}^{(k)}\mathbf{f}^{(0)}(i) \end{aligned} \tag{52}$$

When i takes from 1 to N, it gives equation 51 according to equation 48 and equation 49.Thus we complete the proof.

□

Based on the conclusion of Lemma 4, it is clear that the propagation via p-Laplacian implicit layer admits a scaled non-linear diffusion and two source terms. We note that the form of our non-linear diffusion coincidences to the one developed in (Chen et al., 2022c). However, in (Chen et al., 2022c) the linear operator is assigned via the calculation of graph Laplacian whereas in our model, the transformation acts over the whole p-Laplacian. Finally, it is worth noting that the conclusion in Lemma 4 can be transferred to the implicit schemes[10]. We omit it here.

Remark 6. With sufficiently large μ or small p, one can check that the strength of the diffusion, i.e. $\mathrm{div}(\|\nabla \mathbf{F}^{(k)}\|^{p-2}\nabla \mathbf{F}^{(k)})$, is diluted. Once two source terms $2\mu\boldsymbol{\alpha}^{(k)}\mathbf{DF}^{(k)} + 2\mu\alpha^{(k)}\mathbf{F}^{(0)}$ dominant the whole process, the generated node features approach to $\mathbf{DF^{(k)}} + \mathbf{F}^{(0)}$, which suggests a framelet together with two source terms. Therefore, the energy of the remaining node features in this case is just with the form presented in equation 42. This observation suggests our conclusion on the energy behavior of pL-UFG (Proposition 2); the interaction within pL-UFG described in Lemma 3 and Corollary 1 can be unified and eventually forms a well defined framework in assessing and understanding the property of pL-UFG.

4 Experiment

Experiment outlines In this section, we present comprehensive experimental results on the claims that we made from the theoretical aspects of our model. All experiments were conducted in PyTorch on NVIDIA Tesla V100 GPU with 5,120 CUDA cores and 16GB HBM2 mounted on an HPC cluster. In addition, for the sake of convenience, we listed the summary of each experimental section as follows:

- In Section 4.1, we show how a sufficient large/small μ can affect model's performance on heterophilic/homophilic graphs, and the results are almost invariant to the choice of p.
- In Section 4.2 we show some tests regarding to the results (i.e., Corollary 2 and Lemma 3) of model's dynamics. Specifically, we verified the conclusions of stronger LFD and HFD in Section 3.3 with controlled model dynamics (quantity of θ) of framelet to illustrate how the p-Laplacian based implicit layer interact with framelet model.
- In Section 4.3 we test the performances of pL-UFG-LFD and pL-UFG-HFD via real-world graph benchmarks versus various baseline models. Furthermore, as these two controllable pL-UFG models largely reduced the computational cost (as we claimed in Section 3.4), we show pL-UFG-LFD and pL-UFG-HFD can even handle the large-scale graph datasets and achieve remarkable learning accuracies.

4.1 Synthetic Experiment on Variation of μ

Setup In this section, we show how a sufficiently large/small of μ can affect model's performance on hetero/homophilic graphs. In order to make a fair comparison, all the parameters of pL-UFG followed the settings included in (Shao et al., 2022). For this test, we selected two synthetic homo/heterophily datasets: `Cora` (heterophilic index: 0.825, 2708 nodes and 5278 edges) and `Wisconsin` (heterophilic index: 0.15, 499 nodes and 1703 edges) from `https://www.pyg.org/`. We assigned the quantity of $p = \{1, 1.5, 2, 2.5\}$ combined with a set of $\mu = \{0.1, 0.5, 1, 5, 10, 20, 30, 50, 70\}$. The number of epochs was set to 200 and the test accuracy (in %) is obtained as the average test accuracy of 10 runs.

Results and Discussion The experimental results are presented in Figure 2. When examining the results obtained through the homophily graph (Figure 2a), it is apparent that all variants of pL-UFGs achieved the best performance when $\mu = 0.1$, which is the minimum value of μ. As the value of μ increased, the learning accuracy decreased. This suggests that a larger sharpening effect was induced by the model, as stated in Corollary 2 and Proposition 2, causing pL-UFGs to incorporate higher amounts of Dirichlet energy into their generated node features. Consequently, pL-UFGs are better suited for adapting to heterophily graphs.

[10]With a duplication of terminology, here the term "implicit" refers to the implicit scheme (i.e., backward propagation) in the training of the diffusion model.

This observation is further supported by the results in Figure 2b, where all pL-UFG variants achieved their optimal performance with a sufficiently large μ when the input graph is heterophilic.

Additional interesting observation on the above result is despite the fact that all model variants demonstrated superior learning outcomes on both homophilic and heterophilic graphs when assigned sufficiently large or small values of μ, it can be observed that when the quantity of p is small, pL-UFG requires a smaller value of μ to fit the heterophily graph (blue line in Fig. 2b). On the other hand, when the models have relatively large value of p (i.e., $p = 2.5$), it is obvious that these models yielded the most robust results when there is an increase of μ (red line in Fig. 2a). These phenomena further support the notion that p and μ exhibit opposite effects on the model's energy behavior as well as its adaptation to homophily and heterophily graphs.

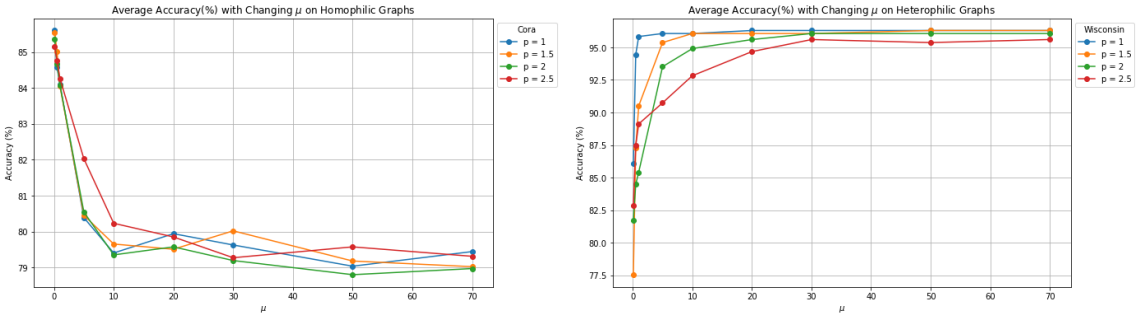

(a) Accuracy on `Cora` via different combinations of μ and p.

(b) Accuracy on `Wisconsin` via different combinations of μ and p.

Figure 2: Performance of pL-UFG with various combinations of the values of μ and p.

4.2 Synthetic Experiment on Testing of Model's Dynamics

Now, we take one step ahead. Based on Lemma 3 and Corollary 2, with the settings of θ provided in Proposition 3, the inclusion of p-Laplacian based implicit layer can further enhance framelet's LFD and HFD dynamics. This suggests that one can control the entries of θ based on the conditions provided in Proposition 3 and by only changing the quantity of μ and p to test model's adaption power on both homophily and heterophily graphs. Therefore, in this section, we show how a (dynamic) controlled framelet model can be further enhanced by the assistant from the p-Laplacian regularizer. Similarly, we applied the same setting to the experiments in (Shao et al., 2022).

Setup and Results To verify the claims on in Lemma 3 and Corollary 2, we deployed the same settings mentioned in Proposition 3. Specifically, we utilized Haar frame with $\ell = 1$ and set $\boldsymbol{\theta}_{0,1} = \mathbf{I}_N$, $\boldsymbol{\theta}_{0,1} = \theta\mathbf{I}_N$. For heterophilic graphs (`Wisconsin`), $\theta = 2$, and for the homophilic graph (`Cora`), $\theta = 0.2$. The result of the experiment is presented in Figure 3. Similar to the results observed from Section 4.1, it is shown that when the relatively large quantity of μ is assigned, model's capability of adapting to homophily/heterophily graph decreased/increased. This directly verifies that the p-Laplacian based implicit layer interacts and further enhances the (controlled) dynamic of the framelet by the value of p and μ, in terms of adaptation.

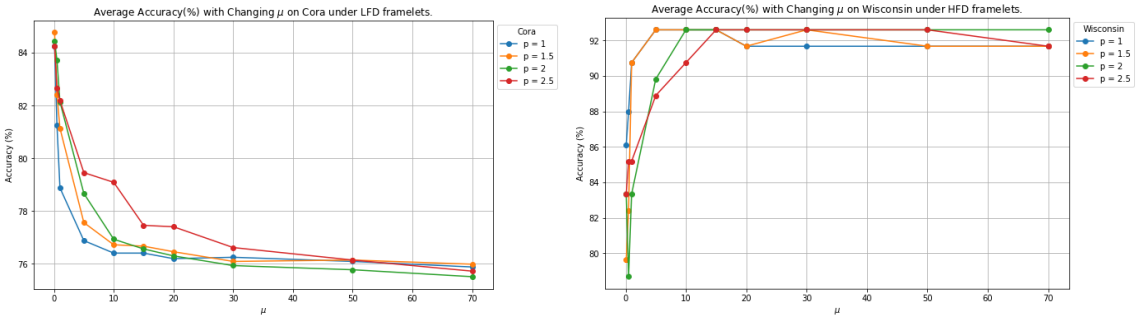

(a) Accuracy on `Cora`

(b) Accuracy on `Wisconsin`

Figure 3: Average Accuracy(%) with Changing μ and p under (manually fixed) LFD/HFD framelet models. All framelet model in Fig. 3a are LFD dynamic with $\theta_{0,1} = \mathbf{I}_N$, $\theta_{1,1} = \theta\mathbf{1}_N$, $\theta = 0.2$. On Fig. 3b, all framelet models are HFD with $\theta_{0,1} = \mathbf{I}_N$, $\theta_{1,1} = \theta\mathbf{1}_N$, $\theta = 2$.

4.3 Real-world Node Classification and Scalability

Previous synthetic numerical results show predictable performance of both pL-UFG-LFD and pL-UFG-HFD. In this section, we present the learning accuracy of our proposed models via real-world homophily and heterophily graphs. Similarly, we deployed the same experimental setting from Shao et al. (2022). In addition, to verify the claim in Remark 3.4, we tested our proposed model via large-scale graph dataset (`ogbn-arxiv`) to show the proposed model's scalability which is rarely explored. We include the summary statistic of the datasets in Table 2. All datasets are split according to Hamilton et al. (2017).

For the settings of μ, p and θ within pL-UFG-LFD and pL-UFG-HFD, we assigned $\mu = \{0.1, 0.5, 1, 2.0\}$, $p = \{1, 1.5, 2, 2.5\}$ and $\theta = \{0.2, 0.5, 0.8\}$ for pL-UFG-LFD in order to fit the homophily graphs, and for pL-UFG-HFD, we assigned $\mu = \{10, 20, 30\}$, $p = \{1, 1.5, 2, 2.0, 2.5\}$ and $\theta = \{5, 7.5, 10\}$ for heterophily graphs. The learning accuracy are presented in Table 3 and 4. We include a brief introduction on the baseline models used in this experiment:

- **MLP**: Standard feedward multiple layer perceptron.
- **GCN** Kipf & Welling (2016): GCN is the first of its kind to implement linear approximation to spectral graph convolutions.
- **SGC** Wu et al. (2019b): SGC reduces GCNs' complexity by removing nonlinearities and collapsing weight matrices between consecutive layers. Thus serves as a more powerful and efficient GNN baseline.
- **GAT** Veličković et al. (2018): GAT generates attention coefficient matrix that element-wisely multiplied on the graph adjacency matrix according to the node feature based attention mechanism via each layer to propagate node features via the relative importance between them.
- **JKNet** Xu et al. (2018b): JKNet offers the capability to adaptively exploit diverse neighbourhood ranges, facilitating enhanced structure-aware representation for individual nodes.
- **APPNP** Gasteiger et al. (2019): APPNP leverages personalized PageRank to disentangle the neural network from the propagation scheme, thereby merging GNN functionality.
- **GPRGNN** Chien et al. (2021): The GPRGNN architecture dynamically learns General Pagerank (GPR) weights to optimize the extraction of node features and topological information from a graph, irrespective of the level of homophily present.
- **p-GNN** Fu et al. (2022):p-GNN is a p-Laplacian based graph neural network model that incorporates a message-passing mechanism derived from a discrete regularization framework. To make a fair comparison, we test p-GNN model with different quantity of p.

- **UFG** Zheng et al. (2022): UFG, a class of GNNs built upon framelet transforms utilizes framelet decomposition to effectively merge graph features into low-pass and high-pass spectra.
- **pL-UFG** Shao et al. (2022): pL-UFG employs a p-Laplacian based implicit layer to enhance the adaptability of multi-scale graph convolution networks (i.e.,UFG) to filter-based domains, effectively improving the model's adaptation to both homophily and heterophily graphs. Furthermore, as two types of pL-UFG models are proposed in Shao et al. (2022), we test both two pL-UFG variants as our baseline models. For more details including the precise formulation of the model, please check Shao et al. (2022).

Table 2: Statistics of the datasets, $\mathcal{H}(\mathcal{G})$ represent the level of homophily of overall benchmark datasets.

Datasets	Class	Feature	Node	Edge	$\mathcal{H}(\mathcal{G})$
Cora	7	1433	2708	5278	0.825
CiteSeer	6	3703	3327	4552	0.717
PubMed	3	500	19717	44324	0.792
Computers	10	767	13381	245778	0.802
Photo	8	745	7487	119043	0.849
CS	15	6805	18333	81894	0.832
Physics	5	8415	34493	247962	0.915
Arxiv	23	128	169343	1166243	0.681
Chameleon	5	2325	2277	31371	0.247
Squirrel	5	2089	5201	198353	0.216
Actor	5	932	7600	26659	0.221
Wisconsin	5	251	499	1703	0.150
Texas	5	1703	183	279	0.097
Cornell	5	1703	183	277	0.386

Discussion on the Results, Scalability and Computational Complexity From both Table 3 and 4, it is clear that our proposed model (pL-UFG-LFD and pL-UFG-HFD) produce state-of-the-art learning accuracy compared to various baseline models. For the datasets (i.e.,`Pubmed` and `Squirrel`) on which pL-UFG-LFD and pL-UFG-HFD are not the best, one can observe that pL-UFG-LFD and pL-UFG-HFD still have nearly identical learning outcomes compared to the best pL-UFG results. This suggests even within the pL-UFG with controlled framelet dynamics, by adjusting the values of μ and p, our proposed models are still able to generate state-of-the-art learning results with the computational complexity largely reduced compared to the pL-UFG and UFG. This observation directly verifies Lemma 3 and Corollary 2. In addition, due to the reduction of computational cost, our dynamic controlled models (pL-UFG-LFD and pL-UFG-HFD) show a strong capability of handling the large-scale graph dataset, which is a challenging issue (scalability) for some GNNs especially multi-scale graph convolutions such as framelets (Zheng et al., 2022) without additional data pre-processing steps. Accordingly, one can check that pL-UFG-LFD outperforms all included baselines on `Arxiv` datasets.

4.4 Limitation of the Proposed Models and Future Studies

First, we note that our analysis on the convergence, energy dynamic and equivalence between our proposed model can be applied or partially applied to most of existing GNNs. Based on we have claimed in regarding to the theoretical perspective of pL-UFG, although we assessed model property via different perspective, eventually all theoretical conclusions come to the same conclusion (i.e., the asymptotic behavior of pL-UFG). Therefore, it would be beneficial to deploy our analyzing framework to other famous GNNs. Since the main propose of this paper is to re-assess the property of pL-UFG, we leave this to the future work.

In addition, to induce LFD/HFD to pL-UFG, we set the value of θ as constant according to Proposition 3, however, due to large variety of real-world graphs, it is challenging to determine the most suitable θ when we fix it as a constant. This suggests the exploration on controlling model's dynamic via selecting θ is still

Table 3: Test accuracy (%) on homophilic graphs, the highest learning accuracy are highlighted in **bold**. The term OOM means out of memory.

Method	Cora	CiteSeer	PubMed	Computers	Photos	CS	Physics	Arxiv
MLP	66.04±1.11	68.99±0.48	82.03±0.24	71.89±5.36	86.11±1.35	93.50±0.24	94.56±0.11	36.44±0.78
GCN	84.72±0.38	75.04±1.46	83.19±0.13	78.82±1.87	90.00±1.49	93.00±0.12	95.55±0.09	47.18± 0.79
SGC	83.79±0.37	73.52±0.89	75.92±0.26	77.56±0.88	86.44±0.35	92.18±0.22	94.99±0.13	48.10± 0.30
GAT	84.37±1.13	74.80±1.00	83.92±0.28	78.68±2.09	89.63±1.75	92.57 ±0.14	95.13±0.15	OOM
JKNet	83.69±0.71	74.49±0.74	82.59±0.54	69.32±3.94	86.12±1.12	91.11±0.22	94.45±0.33	OOM
APPNP	83.69±0.71	75.84±0.64	80.42±0.29	73.73±2.49	87.03±0.95	91.52±0.14	94.71±0.11	38.97± 0.81
GPRGNN	83.79±0.93	75.94±0.65	82.32±0.25	74.26±2.94	88.69±1.32	91.89 ±0.08	94.85±0.23	37.64±1.67
UFG	80.64±0.74	73.30±0.19	81.52±0.80	66.39±6.09	86.60±4.69	95.27±0.04	95.77±0.04	OOM
$\text{PGNN}^{1.0}$	84.21±0.91	75.38±0.82	84.34±0.33	81.22±2.62	87.64±5.05	94.88±0.12	96.15±0.12	OOM
$\text{PGNN}^{1.5}$	84.42±0.71	75.44±0.98	84.48±0.21	82.68±1.15	91.83±0.77	94.13±0.08	96.14±0.08	OOM
$\text{PGNN}^{2.0}$	84.74±0.67	75.62±1.07	84.25 ±0.35	83.40±0.68	91.71±0.93	94.28±0.10	96.03±0.07	OOM
$\text{PGNN}^{2.5}$	84.48±0.77	75.22±0.73	83.94±0.47	82.91±1.34	91.41±0.66	93.40±0.07	95.75±0.05	OOM
$\text{pL-UFG1}^{1.0}$	84.54±0.62	75.88±0.60	85.56±0.18	82.07±2.78	85.57±19.92	95.03±0.22	96.19±0.06	47.71±9.13
$\text{pL-UFG1}^{1.5}$	84.96±0.38	76.04±0.85	85.59±0.18	85.04±1.06	92.92±0.37	95.03±0.22	96.27±0.06	48.75±8.37
$\text{pL-UFG1}^{2.0}$	85.20±0.42	76.12±0.82	85.59± 0.17	85.26±1.15	92.65±0.65	94.77±0.27	96.04±0.07	OOM
$\text{pL-UFG1}^{2.5}$	85.30±0.60	76.11±0.82	85.54±0.18	85.18±0.88	91.49±1.29	94.86±0.14	95.96±0.11	OOM
$\text{pL-UFG2}^{1.0}$	84.42±0.32	74.79± 0.62	85.45±0.18	84.88±0.84	85.30±19.50	95.03±0.19	96.06±0.11	47.77±7.28
$\text{pL-UFG2}^{1.5}$	85.60±0.36	75.61±0.60	85.59±0.18	84.55±1.57	93.00±0.61	95.03±0.19	96.14±0.09	47.92±6.19
$\text{pL-UFG2}^{2.0}$	85.20±0.42	76.12±0.82	**85.59±0.17**	85.27±1.15	92.50±0.40	94.77±0.27	96.05± 0.07	OOM
pL-UFG-LFD	**85.64±1.36**	**77.39±1.59**	85.08±1.33	**85.36±1.39**	**93.17±1.30**	**96.13±1.08**	**96.49±1.04**	**49.79±2.31**

rough. Moreover, based on Definition 1, the homophily index of a graph is summary statistic over all nodes. However, even in the highly homophilic graph, there are still some nodes with their neighbours with different labels. This suggests the index is only capable of presenting the global rather than local labelling information of the graph. Accordingly, assigning a constant θ to induce LFD/HFD might not be able to equip pL-UFG enough power to capture detailed labelling information of the graph. Therefore, another future research direction is to potentially explore the design of θ via the local labelling information of the graph.

5 Concluding Remarks

In this work, we performed theoretical analysis on pL-UFG. Specifically, we verified that by choosing suitable quantify of the model parameters (μ and p), the implicit propagation induced from p-Laplacian is capable of amplifying or shrinking the Dirichlet energy of the node features produced from the framelet. Consequently, such manipulation of the energy results in a stronger energy dynamic of framelet and therefore enhancing model's adaption power on both homophilic and heterophilic graphs. We further explicitly showed the proof of the convergence of pL-UFG, which to our best of knowledge, fills the knowledge gap at least in the field of p-Laplacian based multi-scale GNNs. Moreover, we showed the equivalence between pL-UFG and the non-linear graph diffusion, indicating that pL-UFG can be trained via various training schemes. Finally, it should be noted that for the simplicity of the analysis, we have made several assumptions and only focus on the Haar type frames. It suffices in regards to the scope of this work. However, it would be interesting to consider more complex energy dynamics by reasonably dropping some of the assumptions or from other types of frames, we leave this to future work.

Table 4: Test accuracy (%) on heterophilic graphs. The highest testing accuracy are highlighted in **bold**.

Method	Chameleon	Squirrel	Actor	Wisconsin	Texas	Cornell
MLP	48.82 ± 1.43	34.30 ± 1.13	41.66 ± 0.83	93.45 ± 2.09	71.25 ± 12.99	83.33 ± 4.55
GCN	33.71 ± 2.27	26.19 ± 1.34	33.46 ± 1.42	67.90 ± 8.16	53.44 ± 11.23	55.68 ± 10.57
SGC	33.83 ± 1.69	26.89 ± 0.98	32.08 ± 2.22	59.56 ± 11.19	64.38 ± 7.53	43.18 ± 16.41
GAT	41.95 ± 2.65	25.66 ± 1.72	33.64 ± 3.45	60.65 ± 11.08	50.63 ± 28.36	34.09 ± 29.15
JKNet	33.50 ± 3.46	26.95 ± 1.29	31.14 ± 3.63	60.42 ± 8.70	63.75 ± 5.38	45.45 ± 9.99
APPNP	34.61 ± 3.15	32.61 ± 0.93	39.11 ± 1.11	82.41 ± 2.17	80.00 ± 5.38	60.98 ± 13.44
GPRGNN	34.23 ± 4.09	34.01 ± 0.82	34.63 ± 0.58	86.11 ± 1.31	84.38 ± 11.20	66.29 ± 11.20
UFG	50.11 ± 1.67	31.48 ± 2.05	40.13 ± 1.11	93.52 ± 2.36	84.69 ± 4.87	83.71 ± 3.28
$\text{PGNN}^{1.0}$	49.04 ± 1.16	34.79 ± 1.01	40.91 ± 1.41	94.35 ± 2.16	82.00 ± 11.31	82.73 ± 6.92
$\text{PGNN}^{1.5}$	49.12 ± 1.14	34.86 ± 1.25	40.87 ± 1.47	94.72 ± 1.91	81.50 ± 10.70	81.97 ± 10.16
$\text{PGNN}^{2.0}$	49.34 ± 1.15	34.97 ± 1.41	40.83 ± 1.81	94.44 ± 1.75	84.38 ± 11.52	81.06 ± 10.18
$\text{PGNN}^{2.5}$	49.16 ± 1.40	34.94 ± 1.57	40.78 ± 1.51	94.35 ± 2.16	83.38 ± 12.95	81.82 ± 8.86
$\text{pL-UFG1}^{1.0}$	56.81 ± 1.69	38.81 ± 1.97	41.26 ± 1.66	96.48 ± 0.94	86.13 ± 7.47	86.06 ± 3.16
$\text{pL-UFG1}^{1.5}$	56.89 ± 1.17	39.73 ± 1.22	40.95 ± 0.93	96.48 ± 1.07	87.00 ± 5.16	86.52 ± 2.29
$\text{pL-UFG1}^{2.0}$	56.24 ± 1.02	39.72 ± 1.86	40.95 ± 0.93	96.59 ± 0.72	86.50 ± 8.84	85.30 ± 2.35
$\text{pL-UFG1}^{2.5}$	56.11 ± 1.25	39.38 ± 1.78	41.04 ± 0.99	95.34 ± 1.64	89.00 ± 4.99	83.94 ± 3.53
$\text{pL-UFG2}^{1.0}$	55.51 ± 1.53	36.94 ± 5.69	29.28 ± 19.25	93.98 ± 2.94	85.00 ± 5.27	87.73 ± 2.49
$\text{pL-UFG2}^{1.5}$	57.22 ± 1.19	$\mathbf{39.80 \pm 1.42}$	40.89 ± 0.75	96.48 ± 0.94	87.63 ± 5.32	86.82 ± 1.67
$\text{pL-UFG2}^{2.0}$	56.19 ± 0.99	39.74 ± 1.66	41.01 ± 0.80	96.14 ± 1.16	86.50 ± 8.84	85.30 ± 2.35
$\text{pL-UFG2}^{2.5}$	55.69 ± 1.15	39.30 ± 1.68	40.86 ± 0.74	95.80 ± 1.44	86.38 ± 2.98	84.55 ± 3.31
$\text{pL-fUFG}^{1.0}$	55.80 ± 1.93	38.43 ± 1.26	32.84 ± 16.54	93.98 ± 3.47	86.25 ± 6.89	87.27 ± 2.27
$\text{pL-fUFG}^{1.5}$	55.65 ± 1.96	38.40 ± 1.52	41.00 ± 0.99	96.48 ± 1.29	87.25 ± 3.61	86.21 ± 2.19
$\text{pL-fUFG}^{2.0}$	55.95 ± 1.29	38.33 ± 1.71	41.25 ± 0.84	96.25 ± 1.25	88.75 ± 4.97	83.94 ± 3.78
$\text{pL-fUFG}^{2.5}$	55.56 ± 1.66	38.39 ± 1.48	40.55 ± 0.50	95.28 ± 2.24	88.50 ± 7.37	83.64 ± 3.88
pL-UFG-HFD	$\mathbf{58.60 \pm 1.74}$	39.63 ± 2.01	$\mathbf{44.63 \pm 2.75}$	$\mathbf{96.64 \pm 1.77}$	$\mathbf{89.31 \pm 8.40}$	$\mathbf{88.97 \pm 3.36}$

References

Michael M Bronstein, Joan Bruna, Taco Cohen, and Petar Veličković. Geometric deep learning: Grids, groups, graphs, geodesics, and gauges. *arXiv preprint arXiv:2104.13478*, 2021.

Ben Chamberlain, James Rowbottom, Maria I Gorinova, Michael Bronstein, Stefan Webb, and Emanuele Rossi. Grand: Graph neural diffusion. In *International Conference on Machine Learning*, pp. 1407–1418. PMLR, 2021a.

Benjamin Chamberlain, James Rowbottom, Davide Eynard, Francesco Di Giovanni, Xiaowen Dong, and Michael Bronstein. Beltrami flow and neural diffusion on graphs. In M. Ranzato, A. Beygelzimer, Y. Dauphin, P.S. Liang, and J. Wortman Vaughan (eds.), *Advances in Neural Information Processing Systems*, volume 34, pp. 1594–1609. Curran Associates, Inc., 2021b. URL `https://proceedings.neurips.cc/paper_files/paper/2021/file/0cbed40c0d920b94126eaf5e707be1f5-Paper.pdf`.

Benjamin Paul Chamberlain, James Rowbottom, Davide Eynard, Francesco Di Giovanni, Xiaowen Dong, and Michael M Bronstein. Beltrami flow and neural diffusion on graphs, 2021c. URL `https://arxiv.org/abs/2110.09443`.

Hao Chen, Yu Guang Wang, and Huan Xiong. Lower and upper bounds for numbers of linear regions of graph convolutional networks. *arXiv preprint arXiv:2206.00228*, 2022a.

Jialin Chen, Yuelin Wang, Cristian Bodnar, Pietro Liò, and Yu Guang Wang. Dirichlet energy enhancement of graph neural networks by framelet augmentation. *github*, 2022b.

Jie Chen, Tengfei Ma, and Cao Xiao. FastGCN: Fast learning with graph convolutional networks via importance sampling. In *International Conference on Learning Representations*, 2018. URL https://openreview.net/forum?id=rytstxWAW.

Qi Chen, Yifei Wang, Yisen Wang, Jiansheng Yang, and Zhouchen Lin. Optimization-induced graph implicit nonlinear diffusion. In *International Conference on Machine Learning*, pp. 3648–3661. PMLR, 2022c.

Eli Chien, Jianhao Peng, Pan Li, and Olgica Milenkovic. Adaptive universal generalized pagerank graph neural network. In *Proceedings of International Conference on Learning Representations*, 2021.

Fan RK Chung. *Spectral graph theory*, volume 92. American Mathematical Soc., 1997.

Zhiyong Cui, Kristian Henrickson, Ruimin Ke, and Yinhai Wang. Traffic graph convolutional recurrent neural network: A deep learning framework for network-scale traffic learning and forecasting. *IEEE Transactions on Intelligent Transportation Systems*, 21(11):4883–4894, 2019.

Michaël Defferrard, Xavier Bresson, and Pierre Vandergheynst. Convolutional neural networks on graphs with fast localized spectral filtering. *Advances in Neural Information Processing Systems*, 29, 2016.

Francesco Di Giovanni, James Rowbottom, Benjamin P Chamberlain, Thomas Markovich, and Michael M Bronstein. Graph neural networks as gradient flows. *arXiv:2206.10991*, 2022.

Bin Dong. Sparse representation on graphs by tight wavelet frames and applications. *Applied and Computational Harmonic Analysis*, 42(3):452–479, 2017. doi: 10.1016/j.acha.2015.09.005.

David K Duvenaud, Dougal Maclaurin, Jorge Iparraguirre, Rafael Bombarell, Timothy Hirzel, Alán Aspuru-Guzik, and Ryan P Adams. Convolutional networks on graphs for learning molecular fingerprints. *Advances in Neural Information Processing Systems*, 28, 2015.

Guoji Fu, Peilin Zhao, and Yatao Bian. p-Laplacian based graph neural networks. In *Proceedings of the 39th International Conference on Machine Learning*, volume 162 of *PMLR*, pp. 6878–6917, 2022.

Johannes Gasteiger, Aleksandar Bojchevski, and Stephan Günnemann. Predict then propagate: Graph neural networks meet personalized pagerank. In *Proceedings of International Conference on Learning Representations*, 2019.

Justin Gilmer, Samuel S Schoenholz, Patrick F Riley, Oriol Vinyals, and George E Dahl. Neural message passing for quantum chemistry. In *International Conference on Machine Learning*, pp. 1263–1272. PMLR, 2017.

Fangda Gu, Heng Chang, Wenwu Zhu, Somayeh Sojoudi, and Laurent El Ghaoui. Implicit graph neural networks. In H. Larochelle, M. Ranzato, R. Hadsell, M.F. Balcan, and H. Lin (eds.), *Advances in Neural Information Processing Systems*, volume 33, pp. 11984–11995. Curran Associates, Inc., 2020. URL https://proceedings.neurips.cc/paper_files/paper/2020/file/8b5c8441a8ff8e151b191c53c1842a38-Paper.pdf.

Will Hamilton, Zhitao Ying, and Jure Leskovec. Inductive representation learning on large graphs. *Advances in Neural Information Processing Systems*, 30, 2017.

David K Hammond, Pierre Vandergheynst, and Rémi Gribonval. Wavelets on graphs via spectral graph theory. *Applied and Computational Harmonic Analysis*, 30(2):129–150, 2011.

Andi Han, Dai Shi, Zhiqi Shao, and Junbin Gao. Generalized energy and gradient flow via graph framelets. *arXiv preprint arXiv:2210.04124*, 2022.

Mingguo He, Zhewei Wei, Hongteng Xu, et al. Bernnet: Learning arbitrary graph spectral filters via bernstein approximation. *Advances in Neural Information Processing Systems*, 34:14239–14251, 2021.

Thomas N Kipf and Max Welling. Semi-supervised classification with graph convolutional networks. *arXiv preprint arXiv:1609.02907*, 2016.

Ming Li, Zheng Ma, Yu Guang Wang, and Xiaosheng Zhuang. Fast Haar transforms for graph neural networks. *Neural Networks*, 128:188–198, 2020.

Qimai Li, Zhichao Han, and Xiao-Ming Wu. Deeper insights into graph convolutional networks for semi-supervised learning. In *AAAI Conference on Artificial Intelligence*, 2018.

Juncheng Liu, Kenji Kawaguchi, Bryan Hooi, Yiwei Wang, and Xiaokui Xiao. Eignn: Efficient infinite-depth graph neural networks. *Advances in Neural Information Processing Systems*, 34:18762–18773, 2021.

Christopher Morris, Martin Ritzert, Matthias Fey, William L Hamilton, Jan Eric Lenssen, Gaurav Rattan, and Martin Grohe. Weisfeiler and leman go neural: Higher-order graph neural networks. In *Proceedings of the AAAI conference on artificial intelligence*, volume 33, pp. 4602–4609, 2019.

Remigijus Paulavičius and Julius Žilinskas. Analysis of different norms and corresponding lipschitz constants for global optimization. *Technological and Economic Development of Economy*, 12(4):301–306, 2006.

Zhiqi Shao, Andi Han, Dai Shi, Andrey Vasnev, and Junbin Gao. Generalized Laplacian regularized framelet gcns. *arXiv:2210.15092*, 2022.

Wim Sweldens. The lifting scheme: A construction of second generation wavelets. *SIAM Journal on Mathematical Analysis*, 29(2):511–546, 1998. doi: 10.1137/S0036141095289051.

Matthew Thorpe, Tan Minh Nguyen, Hedi Xia, Thomas Strohmer, Andrea Bertozzi, Stanley Osher, and Bao Wang. GRAND++: Graph neural diffusion with a source term. In *International Conference on Learning Representations*, 2022. URL `https://openreview.net/forum?id=EMxu-dzvJk`.

Petar Veličković, Guillem Cucurull, Arantxa Casanova, Adriana Romero, Pietro Liò, and Yoshua Bengio. Graph attention networks. In *International Conference on Learning Representations*, 2018.

Jingyi Wang and Zhidong Deng. A deep graph wavelet convolutional neural network for semi-supervised node classification. In *2021 International Joint Conference on Neural Networks (IJCNN)*, pp. 1–8. IEEE, 2021.

Xiyuan Wang and Muhan Zhang. How powerful are spectral graph neural networks. In *International Conference on Machine Learning*, pp. 23341–23362. PMLR, 2022.

Yifei Wang, Yisen Wang, Jiansheng Yang, and Zhouchen Lin. Dissecting the diffusion process in linear graph convolutional networks. *Advances in Neural Information Processing Systems*, 34:5758–5769, 2021.

Felix Wu, Amauri Souza, Tianyi Zhang, Christopher Fifty, Tao Yu, and Kilian Weinberger. Simplifying graph convolutional networks. In *International Conference on Machine Learning*, pp. 6861–6871. PMLR, 2019a.

Felix Wu, Tianyi Zhang, Amauri Holanda de Souza, Christopher Fifty, Tao Yu, and Kilian Q. Weinberger. Simplifying graph convolutional networks. In *Proceedings of International Conference on Machine Learning*, 2019b.

Zonghan Wu, Shirui Pan, Fengwen Chen, Guodong Long, Chengqi Zhang, and S Yu Philip. A comprehensive survey on graph neural networks. *IEEE transactions on Neural Networks and Learning Systems*, 32(1): 4–24, 2020.

Bingbing Xu, Huawei Shen, Qi Cao, Yunqi Qiu, and Xueqi Cheng. Graph wavelet neural network. In *International Conference on Learning Representations*, 2018a.

Keyulu Xu, Chengtao Li, Yonglong Tian, Tomohiro Sonobe, Ken-ichi Kawarabayashi, and Stefanie Jegelka. Representation learning on graphs with jumping knowledge networks. In *Proceedings of International Conference on Machine Learning*, 2018b.

Keyulu Xu, Weihua Hu, Jure Leskovec, and Stefanie Jegelka. How powerful are graph neural networks? In *International Conference on Learning Representations*, 2019. URL `https://openreview.net/forum?id=ryGs6iA5Km`.

Mengxi Yang, Xuebin Zheng, Jie Yin, and Junbin Gao. Quasi-framelets: Another improvement to graph neural networks. *arXiv:2201.04728*, 2022.

Xuebin Zheng, Bingxin Zhou, Junbin Gao, Yuguang Wang, Pietro Lió, Ming Li, and Guido Montufar. How framelets enhance graph neural networks. In *International Conference on Machine Learning*, pp. 12761–12771. PMLR, 2021.

Xuebin Zheng, Bingxin Zhou, Yu Guang Wang, and Xiaosheng Zhuang. Decimated framelet system on graphs and fast g-framelet transforms. *Journal of Machine Learning Research*, 23:18–1, 2022.

Xuebin Zheng, Bingxin Zhou, Ming Li, Yu Guang Wang, and Junbin Gao. Mathnet: Haar-like wavelet multiresolution analysis for graph representation learning. *Knowledge-Based Systems*, 273:110609, 2023. ISSN 0950-7051. doi: https://doi.org/10.1016/j.knosys.2023.110609. URL `https://www.sciencedirect.com/science/article/pii/S0950705123003593`.

Bingxin Zhou, Ruikun Li, Xuebin Zheng, Yu Guang Wang, and Junbin Gao. Graph denoising with framelet regularizer. *arXiv:2111.03264*, 2021.

Bingxin Zhou, Xinliang Liu, Yuehua Liu, Yunying Huang, Pietro Lio, and Yu Guang Wang. Well-conditioned spectral transforms for dynamic graph representation. In *The First Learning on Graphs Conference*, 2022. URL `https://openreview.net/forum?id=kQsniwmGgF5`.

Dengyong Zhou and Bernhard Schölkopf. Regularization on discrete spaces. In *Joint Pattern Recognition Symposium*, pp. 361–368. Springer, 2005.

Jiong Zhu, Yujun Yan, Lingxiao Zhao, Mark Heimann, Leman Akoglu, and Danai Koutra. Beyond homophily in graph neural networks: Current limitations and effective designs. In *Advances in Neural Information Processing Systems*, volume 33, pp. 7793–7804, 2020.

Chunya Zou, Andi Han, Lequan Lin, and Junbin Gao. A simple yet effective SVD-GCN for directed graphs. *arXiv:2205.09335*, 2022.